

Emergence of brain function from structure: an algebraic quantum model

Elkaïoum M. Moutuou^{1,*} and Habib Benali¹

¹*Department of Electrical and Computer Engineering,
Concordia University, Montreal, QC, H3G 1M8*

A fundamental paradigm in neuroscience is that cognitive functions – such as perception, learning, memory, and locomotion – are governed by the brain’s structural organization. Yet, the theoretical principles explaining how the physical architecture of the nervous system shapes its function remain elusive. Here, we combine concepts from quantum statistical mechanics and graph C^* -algebras to introduce a theoretical framework where functional states of a structural connectome emerge as thermal equilibrium states of the underlying directed network. These equilibrium states, defined from the Kubo–Martin–Schwinger states formalism (KMS states), quantify the relative contribution of each neuron to the information flow within the connectome. Using the prototypical connectome of the nematode *Caenorhabditis elegans*, we provide a comprehensive description of these KMS states, explore their functional implications, and establish the predicted functional network based on the nervous system’s anatomical connectivity. Ultimately, we present a model for identifying the potential functional states of a detailed structural connectome and for conceptualizing the structure-function relationship.

INTRODUCTION

A core tenet of *connectomics* in neuroscience is that brain functions emerge from contextual collective properties of its structural substrates [5, 25, 32]. It emphasizes the importance of the brain’s structural network, or the *connectome* [21, 65, 66], in determining how information is processed, integrated, and transmitted within such a complex system. Based on this premise, exploring the relationships between the structure of the brain’s wiring systems and the flow of information across synaptic circuitries has the potential to provide deeper insights into how neuronal assemblies [16, 56] underpin cognition, behavior, neurological and psychiatric states [24, 79]. This perspective has fueled intense research over the past few decades, aimed at: (i) producing comprehensive maps that detail the anatomical connections between neural units at various levels—from macroscale networks of brain regions and white matter pathways using neuroimaging techniques [9, 22] to microscale synaptic circuits using high-resolution imaging technologies such as electron microscopy [19, 72, 73, 75, 76]—and (ii) developing quantitative models for understanding how these complex architectures contribute to brain functions and dysfunctions [11, 27, 48, 52, 64].

Large-scale connectomics data have been generated across a wide array of species—such as *C. elegans* [73], *Drosophila* [75], *Platynereis dumerilii* [72], mice [1] and humans [62]—and interdisciplinary research, particularly the application of graph theory and network science, has been pivotal in analyzing these datasets, modeling the interactions and information flow in neural circuits, and detecting connectivity patterns crucial for understanding the functional states of the nervous system [16, 50].

With its 302 neurons and approximately 13,000 chemical and electrical synapses, the *C. elegans* synaptic connectome is the most complete of these endeavors [19, 71, 73].

It has served as a prototypical nervous system for building sophisticated models to uncover specific neural circuits underlying complex behaviors and predict brain dysfunctions based on structural patterns [50, 78].

While these efforts have provided new perspectives on the structural mechanisms underlying cognition, a theoretical framework describing how the brain’s physical architecture shapes and predicts its function is still lacking. Here, we address this problem by combining quantum statistical mechanics with graph C^* -algebras to develop the repertoire of functional networks predicted from the structure of the *C. elegans* somatic connectome [19, 71].

Specifically, we introduce a mathematical formalism in which functional states of a connectome are represented by the thermal equilibrium states of the underlying directed network; i.e., the directed graph whose nodes are the neurons and edges are synapses and gap-junctions. The concept of thermal equilibrium states we present here for directed networks is motivated by graph algebras [20, 45, 58] and the mathematical formulation of the theory of *Kubo–Martin–Schwinger* (KMS) states [30, 34].

Quantum statistical mechanics deals with the thermodynamical properties of large systems with infinitely many degrees of freedom, and such a system is formally represented by a C^* -*dynamical system*: a C^* -algebra together with a dynamics; that is, an algebra of bounded operators on a Hilbert space with a group action representing the time evolution of the system [13, 14, 35, 77]. Elements of this C^* -algebra are the observables of the system, and its time-invariant states are derived from the KMS equations and correspond to the thermal equilibrium of the system at given inverse temperatures. In particular, when the Hilbert space is finite-dimensional, the corresponding C^* -algebra is a matrix algebra $M_n(\mathbb{C})$, the dynamics is defined by a Hamiltonian H through the formula $e^{itH} A e^{-itH}$ for $A \in M_n(\mathbb{C})$, and the equilibrium states of the system at *inverse temperature* β are the Gibbs states $\text{Tr}(e^{-\beta H} A) / \text{Tr}(e^{-\beta H})$ [14] (see Appendix A

* elkaïoum.moutuou@concordia.ca

for details).

Now, modeling the synaptic connectome as a directed network G with parallel edges and self-loops generates an infinite system \mathcal{O}_G encompassing all possible information flow pathways, including infinitely many feedback loops within G . More precisely, \mathcal{O}_G is the the *graph C*-algebra* (also called the *Toeplitz algebra*) of G [7, 45, 58], which is an abstract infinite space encoding topological and combinatorial properties of all directed walks in the graph. Moreover, this C*-algebra carries a natural dynamics making it a C*-dynamical system, and from a fundamental result of an Huef et al. [3], the KMS states of this system translates into probability distributions on G satisfying certain conditions (see Appendix B). Following this relation, we define the KMS states of the connectome as specific distributions that measure the neuronal connectivity states and quantify the information flow pathways between each pair of neurons. We then present a complete description of these equilibrium states and discuss their functional implications.

Specifically, we show that at a fixed inverse temperature each neuron generates a *pure state* –referred to as the '*neural emittance profile*' (NEP)– that captures the potential 'functional' connectivity networks of each individual neuron. We illustrate how these profiles vary with inverse temperature and define the *structure-function divergence* to quantify the extent to which they deviate from anatomical structure. Furthermore, we demonstrate that the NEPs of all neurons form the foundation of all other KMS states, from which we extract two fundamental features that characterize the functional organization of the *C. elegans* nervous system: (i) the *pure functional connectome* of the nematode, which is the whole functional atlas predicted and driven by its anatomical network, and (ii) an *integration capacity* (IC) index that measures the degree to which neurons are able to integrate multiple independent flows of information.

Ultimately, the quantum model we present here offers a theoretical framework for decoding the structure-function relationship, thereby revealing neuronal assemblies that mediate sensorimotor processing to trigger complex behaviors such as thermotaxis [43, 49], mechanosensation [40], and locomotion [12, 17, 73].

RESULTS

1. State vectors and structural connectivity of a directed connectome. We model a structural connectome as a directed graph $G = (V, E)$ with parallel edges and self-loops; the node set V represents the neurons, and the edge set E consists of the chemical and electrical synapses (gap junctions). The *source* $s(e)$ and *range* $r(e)$ of an edge are respectively the pre- and post-synaptic neurons of the synapse. As a prototypical connectome model, we use the somatic nervous system of the adult hermaphrodite *C. elegans* consisting of $N = 280$ individual neurons and $\#E = 12071$ unique chemical and electrical connections

constructed from the old [2, 71, 73] and the newly revised datasets [19] (see Methods for details). Since gap junctions allow bidirectional transmission between neurons, they are represented by reciprocal edges. Our work being focused on investigating the potential functional interactions among neurons through anatomical pathways, we consider both chemical and electrical synapses within a unified wiring system, since both transmission modalities are known to maintain close functional interactions [53] (the resulting network edgelist can be found in Supplementary Data 1).

A (directed) *walk* or *path* \mathbf{e} is a sequence (e_1, \dots, e_n) of edges such that $s(e_i) = r(e_{i+1})$. We use bold letters \mathbf{e}, \mathbf{f} , etc. for directed walks. The length $|\mathbf{e}|$ of \mathbf{e} is the number n of edges composing it, and we set $s(\mathbf{e}) = s(e_n)$ and $r(\mathbf{e}) = r(e_1)$ to be its source and range, respectively. \mathbf{e} is a *cycle* if $s(\mathbf{e}) = r(\mathbf{e})$. The set of all finite walks in G is denoted by $W(G)$.

A (*connectivity*) *state vector* on G is any probability distribution \mathcal{X} on V such that, for $u \in V$, \mathcal{X}_u represents a probability of upstream connectivity of the neuron u . We then say the number \mathcal{X}_u is the *receptance* of u when the *system is in state* \mathcal{X} . The analogy between this definition and the C*-algebraic formulation of quantum mechanics is as follows. Suppose we have a connectivity measure encoding information flow pathways upstream of neurons. These connectivity pathways are random variables, and the associated measures are the *observables* of the system. Then, the system being in state \mathcal{X} means that the expected value of the connectivity into a given neuron u is \mathcal{X}_u . To illustrate this concept, let \mathbf{A} be the *adjacency matrix* of G ; i.e., for two neurons u and v , \mathbf{A}_{uv} is the number of chemical and electrical connections from v to u . Two neurons u and v are *structurally connected* if either $\mathbf{A}_{uv} > 0$ or $\mathbf{A}_{vu} > 0$. Now define the *structural connectivity* of a neuron v as the vector $\mathcal{K}^v = (\mathcal{K}_u^v)_{u \in V} \in [0, 1]^V$ given by

$$\mathcal{K}_u^v = \mathbf{A}_{uv} / k_v^{\text{out}}, \quad (1)$$

where $k_v^{\text{out}} = \sum_w \mathbf{A}_{wv}$ is the number of chemical and electrical connections from v . This is a probability distribution on V that defines a state vector, the *structural connectivity state* of v , which measures the probability of downstream flow of a neuron to its post-synaptic neurons based on the synaptic density; that is, the receptance of a neuron u in this state is the density of electrical and chemical pre-synapses from v if both neurons are structurally connected, and zero otherwise. We can visualize \mathcal{K}^v as a simple directed weighted tree with common internal source node v , where for $u \neq v$, (v, u) is an edge if $\mathcal{K}_u^v > 0$, in which case its weight is $\mathcal{K}_u^v / \sum_{w \neq v} \mathcal{K}_w^v$ (see Methods). For example, in Fig. 1a, we give a schematic visualization of the structural connectivity of the sensory neuron AFDR, while the non-zero values of receptance from AFDR are given in Table I.

2. KMS states of a directed network. One may ask whether the structural connectivity state definition

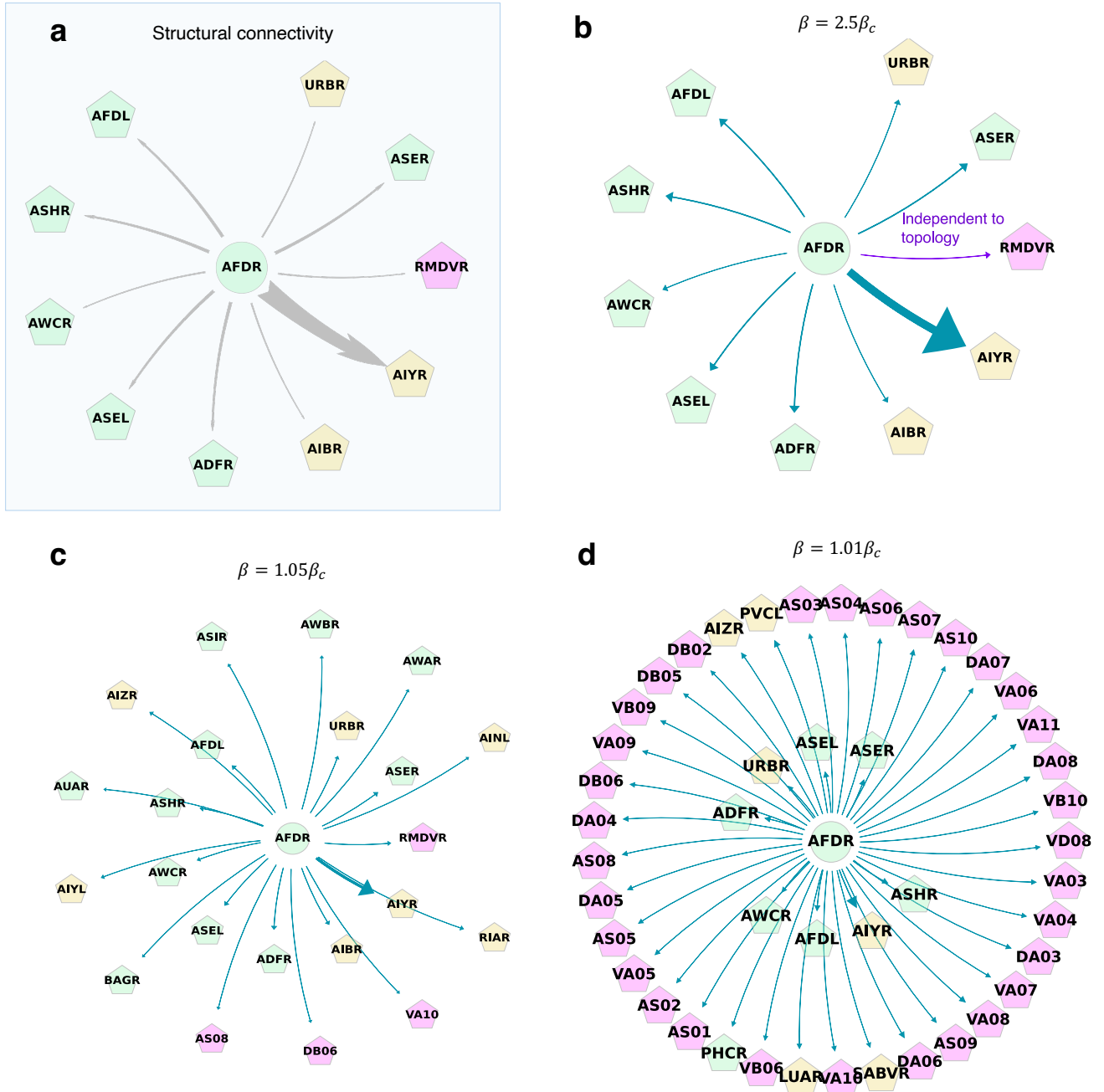


FIG. 1: **Connectivity states of AFDR.** Schematic visualizations of different types of connectivity state vectors AFDR: *structural connectivity* (gray arrows), and the emittance networks (green and purple arrows) obtained from *neural β -emittance profiles* (NEP $_{\beta}$) at different values of inverse temperature $\beta > \beta_c$, where β_c is the critical inverse temperature. **a:** the structural connectivity of AFDR; the weights of the connections are the components of the structural connectivity vector \mathcal{K}^{AFDR} . **b:** At $\beta_s = 2.5\beta_c$, the emittance network coincides with the structural connectivity of AFDR. However, the connection to RMDVR (represented by the purple arrow) is not statistically significant ($p \sim 0.2$), and therefore not a pure functional connection (PFC). In other words, when the system is at this β_s -KMS state, AFDR can functionally communicate only with its direct neighbors, and its functional communications follow the same distribution as its structural connectivity state vector. **c:** At a relatively higher temperature $1/\beta$, long-range communications emerge (i.e. neurons that are not post-synaptic to AFDR, here positioned at the external concentric circle) while the neuron maintains neural emittances onto its direct neighbors (neurons positioned at the internal circle), albeit with lower intensity. **d:** At a very high temperature $1/\beta$ with β close to the critical value, more longer range connections emerge, while some short range ones are either no longer present or not statistically significant. In both c and d, only the PFCs ($p < 0.05$) are considered. Greens are sensory neurons, yellows are interneurons, and pinks are motor neurons.

could be extended to encode long-range pathways from neurons, specifically by working with directed walks in-

stead of edges. However, since, as noted earlier, there might be infinitely many paths from one neuron to another, replacing A_{uv} and κ_v^{out} in (1) with number of paths by simple analogy would lead to non-convergent infinite series, which would give *undefined state vectors*. In order to get a meaningful extension, we first introduce a few concepts.

Given a positive number $\beta > 0$, we say that the system is *at inverse temperature* $\beta > 0$ if the functioning of each connection in the network is affected by a factor of $e^{-\beta}$. The *emittance volume* of v at inverse temperature $\beta = 1/T$ is defined as $\mathcal{Y}_v^\beta = \sum_{e \in W(G), s(e)=v} e^{-\beta|e|}$. This is an infinite series since the connectome contains cycles and self-loops; specifically, 44 neurons have connections onto themselves (such connections are called ‘*autapses*’ in the literature [8, 68]). It represents the volume of all information flow pathways downstream of v when the system is at inverse temperature β . We shall note that similar formulation was used for simple undirected graphs by Katz [41] to measure node status in sociometry, and Estrada and Hatano in [26] to study communicability in undirected complex networks.

Observe that $\mathcal{Y}_v^\beta \geq 1$, reflecting the convention that a node in a graph always emits onto itself through the trivial path of length 0. In particular, if v is not pre-synaptic to any neuron, its emittance volume is 1. Moreover, the series is convergent if $\beta > \log r_G$, where r_G is the spectral radius of G (see Supplementary Note 2 for details). We refer to the value $\beta_c = \log r_G$ as the *critical inverse temperature* of the connectome. In fact, a more practical expression of the emittance volume is obtained in terms of the *adjacency matrix* A of G . Specifically, using a classic result in functional analysis (see Supplementary Note 2), we get

$$\mathcal{Y}_v^\beta = \sum_{u \in V} (1 - e^{-\beta} A)_{uv}^{-1}, \quad (2)$$

for all $\beta > \beta_c$. It follows that $\mathcal{Y}^\beta = (\mathcal{Y}_v^\beta)_{v \in V}$ is a well defined vector in $(1, \infty)^V$ for $\beta > \beta_c$.

Now, we define a β -KMS state of the connectome as a state vector $\mathcal{X} = \mathcal{X}(\Psi)$ that can be obtained from the formula $\mathcal{X} = (1 - e^{-\beta} A)^{-1} \Psi$ where the vector $\Psi \in [0, \infty)^V$ is a solution to the equation

$$\Psi \cdot \mathcal{Y}^\beta = 1. \quad (3)$$

Our definition originates from the theory of KMS states of finite graph C*-algebras [3, 38]. Indeed, from a result of an Huef et al. in [3], solutions of Equation (3) give rise to β -KMS states of the graph C*-algebra of G , and, conversely, every β -KMS state of the latter defines a probability distribution on G obtained from a solution of Equation (3) (see Supplementary Note 2 for details). The set S_β of all β -KMS states of G is a convex space; i.e., if \mathcal{X} and \mathcal{X}' are β -KMS states, then so is $\lambda \mathcal{X} + (1 - \lambda) \mathcal{X}'$ for $0 \leq \lambda \leq 1$. In the next paragraphs, we will describe what KMS states mean in terms of information flow and functional states of the nervous system.

3. Neural emittance profiles as pure states. In the theory of C*-algebras and quantum mechanics, the extreme points of the state space are called *pure states*, and *mixed states* are convex combinations of those [14, 23, 34]. We construct the extreme points of S_β , or the *pure (KMS) states* of the connectome, as follows. For each neuron v and $\beta > \beta_c$, let the vector $\Psi^{v,\beta} \in [0, \infty)^V$ be defined by

$$\Psi_u^{v,\beta} = \begin{cases} 1/\mathcal{Y}_v^\beta, & \text{if } u = v, \\ 0 & \text{otherwise.} \end{cases}$$

It is immediate that $\Psi^{v,\beta}$ is a solution to Equation (3). Hence, for each v and $\beta > \beta_c$, we get a β -KMS state $\mathcal{Z}^{v,\beta}$ by setting $\mathcal{Z}_u^{v,\beta} = \left((1 - e^{-\beta} A)^{-1} \Psi^{v,\beta} \right)_u$, which can simply be expressed as

$$\mathcal{Z}_u^{v,\beta} = \frac{1}{\mathcal{Y}_v^\beta} (1 - e^{-\beta} A)_{uv}^{-1}. \quad (4)$$

We call this quantity the *neural emittance* of v to u at inverse temperature β . It is the probability that information flow from neuron v reach u , when the system is at inverse temperature β . In particular, the *neural self-emittance* $\mathcal{Z}_v^{v,\beta}$ measures the probability of feedback pathways onto neuron v at inverse temperature β . It follows that the distribution $\mathcal{Z}^{v,\beta} = (\mathcal{Z}_u^{v,\beta})_{u \in V}$ is a state vector of the connectome in which the receptance of a neuron u is the the neural emittance of v to u at inverse temperature β . We refer to this state vector as the *neural β -emittance profile* of v or simply the NEP $_\beta$ of v . It quantifies the extent to which v “*functionally*” connects to all the other neurons of the connectome at inverse temperature β . Observe that at larger values of β (lower temperature), $\mathcal{Z}^{v,\beta}$ approaches the Dirac distribution δ^v , where $\delta_v^v = 1$ and $\delta_u^v = 0$ for $u \neq v$. The physical interpretation here is that at very low temperatures (i.e., higher values of β), the outflow connectivity of v freezes into the trivial closed path, and as the temperature increases (i.e., β decreases), its neural emittance widens, first within its close neighborhood at reasonably low temperatures, and at higher temperatures, it expands to long-range communications through possibly infinite number of pathways. More generally, the higher the temperature (β approaches β_c), the more outflow connections emerge from v onto non post-synaptic neurons.

One can visualize these pure states by representing the vector $\mathcal{Z}^{v,\beta}$ as a simple weighted directed star with source node v , where for $u \neq v$, (v, u) is a directed edge of weight $\mathcal{Z}_u^{v,\beta} / \sum_{w \neq v} \mathcal{Z}_w^{v,\beta}$ if $\mathcal{Z}_u^{v,\beta} > 0$, thus obtaining a downstream connectivity network of the neuron consisting of potential functional connections, which we refer to as its *emittance network*.

For instance, Figs.1b–d represent the emittance networks of $v = \text{AFDR}$ at different values of β , illustrating how they evolve as the (inverse) temperature varies. We see that increasing the temperature allows the emergence of long-range emittance connections which are facilitated

by large amounts of parallel pathways of different lengths. Indeed, it is an immediate consequence of formula (4) that parallel paths and redundancies are critical to the emergence of strong neural emittances, and the lengths of pathways and the degree of redundancies that significantly contribute to their weights depend on temperature. More precisely, lower temperatures (i.e., higher values of β) favor parallel direct anatomical connections and short paths. Whereas, higher temperatures enhance the contributions of redundant long pathways of different lengths while lessening the importance of direct anatomical connections in the emittance weights. For example, AFDR has 13 synaptic connections and 52 anatomical paths of length 2 onto the interneuron AIYR, contributing greatly to the important weight of its neural emittance onto the latter at low temperature (Fig.1b). And at higher temperature values, while the neural emittance of AFDR \rightarrow AIYR decreases, other connections are 'established' with neurons onto which AFDR can only be connected through thousands or millions of parallel anatomical paths of length ≥ 2 . For instance, there are 117 paths of length 2 and about 4 millions of length between 3 and 5 linking AFDR to RIAR, contributing to the neural emittance onto this neuron at $\beta = 1.05\beta_c$ (Fig.1c). Similarly, the neural emittance to the ventral cord motor neuron VA11 that appears at $\beta = 1.01\beta_c$ (Fig.1d) is largely due to the more than its 230 million incoming paths of length ≥ 5 from AFDR.

4. Structure-function divergence, structural and functional temperatures. How and to what degree do the emittance networks of a neuron 'differ' from its structural connectivity network. Addressing this question requires an appropriate metric that allows to measure the "divergence" between state vectors. For this aim, we use Uhlmann's *transition probability* between quantum states [37, 69] to define the *structure-function divergence* (**sfd**) of a neuron v as follows:

$$\mathbf{sfd}(v, \beta) = 1 - \left(\sum \left(\mathcal{K}_u^v \mathcal{Z}_u^{v, \beta} \right)^{1/2} \right)^2. \quad (5)$$

Specifically, **sfd** measures how the two networks representing the NEP_β diverges from the anatomical wiring of the neuron in terms of both the number and intensity of their respective connections. Namely, it provides the ratio of non-overlapping receptances in both state vectors. For instance, $\mathbf{sfd}(AS08, \beta) = 0.125$ for $\beta = 1.7\beta_c$ means that, at this inverse temperature, the emittance network of the motor neuron AS08 deviates from anatomy by 12.5%.

Now $\mathbf{sfd}(v, \beta) \sim 0$ if and only if the two distributions $\mathcal{K}^v \sim \mathcal{Z}^{v, \beta}$, which would mean that when the system is at the corresponding β -KMS state $\mathcal{Z}^{v, \beta}$, the neuron can communicate only to its direct neighbors and with the same probabilities as in its structural connectivity state. The value of β that minimizes $\max_v \mathbf{sfd}(v, \beta)$ will be referred to as the *structural (inverse) temperature* of the connectome, and will be denoted by β_s .

We found that at $\beta = 2.5\beta_c$ we have $\mathbf{sfd}(v, \beta) \sim 0$

for each of the 280 neurons. Hence, $\beta_s \approx 10.7394$. In particular, going back to the example of AFDR, its neural β_s -emittance profile has approximately the same receptances as its structural connectivity state. For instance, the structural connection from AFDR to the motor neuron RMDVR has weight $\mathcal{K}_{RMDVR}^{AFDR} = 0.037037$, and its neural emittance onto RMDVR at β_s is $\mathcal{Z}_{RMDVR}^{AFDR, \beta_s} \approx 0.037032$ (see Table I). Namely, the emittance network of AFDR at inverse temperature β_s maps over its anatomical connectivity network.

Studying **sfd** variation of all neurons with respect to inverse temperature, we found that the emittance networks of some neurons, such as the motor neurons DD02, AVAL/R, AS04, remain close to their structural connectivity over long intervals, whereas those of other neurons, such as AS08, the polymodal sensory neurons PVDL/R and FLPL/R, and the interneurons LUAL/R, diverge from structure rapidly after certain low temperature values. For example, at $\beta = 1.7\beta_c$, AVAL and AVAR emittance networks deviate from structure by only 1.3%, while PVDL/R deviate by $\sim 9\%$ and AS08 deviates by 12.5% as mentioned earlier (see Appendix C and Figure 11 for detailed illustrations).

v	u	\mathcal{K}_u^v	$\mathcal{Z}_u^{v, \beta_s}$	p-value
AFDR	ADFR	0.074074	0.074079	0.0006
	ASHR	0.074074	0.074070	0.0002
	URBR	0.037037	0.037031	0.0272
	AIYR	0.481481	0.481441	0.0
	ASEL	0.074074	0.074086	0.0
	AFDL	0.074074	0.074073	0.0002
	ASER	0.074074	0.074087	0.0004
	AIBR	0.037037	0.037061	0.0472
	AWCR	0.037037	0.037040	0.0046
	RMDVR	0.037037	0.037032	0.1806
RMDVR	OLQVL	0.0625	0.062489	0.0002
	SAADL	0.03125	0.031243	0.0066
	SIBDR	0.03125	0.031244	0.0008
	SMBDR	0.03125	0.031244	0.0094
	SAAVR	0.03125	0.031247	0.0056
	CEPDR	0.03125	0.031247	0.002
	RMDVL	0.03125	0.031272	0.0258
	ILIL	0.03125	0.031246	0.0016
	RMDR	0.03125	0.031256	0.0114
	OLQDR	0.03125	0.031248	0.0018
	RIAR	0.03125	0.031259	0.0416
	ILIDR	0.0625	0.062498	0.0
	RMDDL	0.125	0.125003	0.0
	RMDDR	0.03125	0.031255	0.0192
	SMDVR	0.03125	0.031251	0.0116
	SIAVL	0.09375	0.093734	0.0
	SIBVR	0.03125	0.031250	0.0034
	URAVL	0.09375	0.093732	0.0
	AFDR	0.03125	0.031243	0.0056

TABLE I: Neural emittances of AFDR and RMDVR at β_s .

On the other hand, since every $\beta > \beta_c$ generates emittance networks and there is an inverse temperature value β_s around which these networks do not considerably differ

from anatomy (see Figure 9a), which values should we consider 'functionally' interesting enough to work with? To address this question, we examined the *mean total receptance* of the connectome at inverse temperature β ; that is, the average sum of the receptances of a neuron u in the pure states $\mathcal{Z}^{v,\beta}$ for $v \neq u$, which is a number between 0 and 1 (see Methods for the formula). We then consider β as a 'functional' inverse temperature if the mean total receptance is > 0.5 , meaning that at such a β , neurons can receive more from the other neurons than from themselves through self-emittance. By computation we found that the mean total receptance is 0.5 at $\beta_o = 1.07\beta_c$ and > 0.5 on the interval $I_f = (\beta_c, \beta_o)$ (see Appendix C and Figure 9b). For instance, Fig. 1c and Fig. 1d are representation of the emittance networks of AFDR at two different functional inverse temperatures ($1.05\beta_c$ and $1.01\beta_c$, respectively).

5. Dependency on network topology and pure functional connections. It is important to note that emittance networks result from global measures of macroscopic systems consisting of (possibly infinitely) many pathways of various lengths, and they do not provide precise information about the extent to which synaptic circuits are 'important' or 'relevant' to their emergence. More precisely, irrespective of its value, the weight of a connection in the emittance network does not, by itself, allow to know whether the occurrence of this connection is determined by the particular global topology of the anatomical network; i.e., the physical wiring of the connectome. For example, suppose that at a certain value of β the neural emittance of v onto u coincides with an existing direct anatomical link. How can we know whether this particular physical wiring from v to u is 'essential' for a this emittance to emerge at that value of β ? And more generally, how dependent are the NEP_β on the topology of the connectome? To address these questions, we systematically compared the weights in the emittance networks of a given neuron to those that one would get if the network topology was randomly perturbed. Specifically, we measured the likelihood for a neural emittance obtained at a fixed value of β to emerge with equal or larger weight at the same inverse temperature if the synaptic network was randomly rewired (see Methods). Based on their statistical significance, one can then distinguish the emittance connections that are determined by the network topology ($p < .05$) from those that are probably not. In a sense, the former represent the potential functional connections predicted by the network structure of the connectome; we then refer to them as the *pure functional connections* (PFC) of the neuron. For instance, Fig. 1b shows the emittance network of AFDR at the structural inverse temperature β_s , and we found that the emittance onto RMDVR (purple arrow) is not statistically significant ($p \sim .2$, see Table I), therefore not a PFC. On the hand, noting that the anatomical connection from AFDR to RMDVR is defined by a gap-junction, hence a reciprocal connection, prompted us to investigate the structural connectivity along with the emittance network

of RMDVR (Table I) at inverse temperature β_s in order to check whether there is any functional 'asymmetry' on this gap-junction. Interestingly, we found that the neural emittance of RMDVR onto AFDR is a PFC ($p = .0056$, see Table I).

Note that independence of a neural emittance connection on topology is not invariant with (inverse) temperature change. For instance, a PFC from AFDR to RMDVR eventually emerges significantly ($p = .015$) at a functional temperature $\beta_f = 1.05\beta_c$ (Fig. 1c), albeit with lower weight. This apparent discrepancy is a consequence of the fact that the presence of a large volume of redundant anatomical short paths between two neurons increases the likelihood of these neurons to remain 'functionally' connected at low temperature if the system is randomly rewired, and at higher temperature, redundant long-range pathways increases the likelihood of the emittance networks to be less altered by structural rewiring. For instance, there are 1464 anatomical paths of length ≤ 3 all connecting AFDR onto RMDVR, while longer paths between these neurons rely heavily on the existing autapses on RMDVR and other interconnecting neurons such as AFDL, RIAR, IL1DR, etc., forming an infinite number of feedback loops that are very likely destroyed after random reconfiguration of the network.

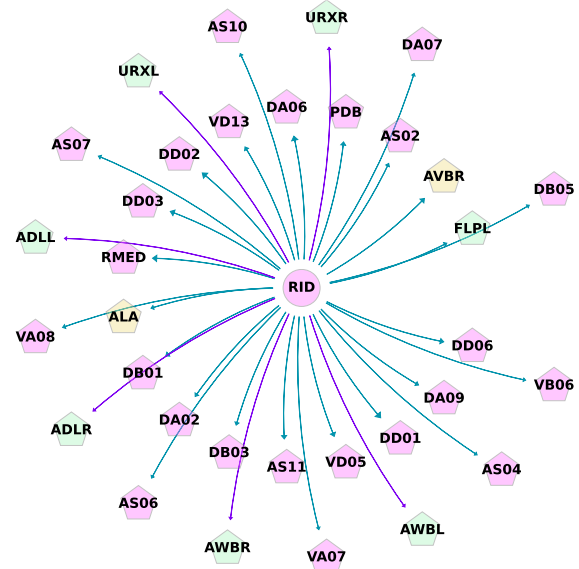


FIG. 2: **Emittance network of RID.** The pink arrows are connections that are not determined by the network topology, that is, the particular anatomical wiring of the neuron, therefore not PFCs. Green arrows are emittance connections that are topology-dependent, therefore PFCs. These connections coincide with the functional connections from RID to the neuron classes URX and ADL that have been identified by Randi et al. to be driven by extrasynaptic signaling.

6. Non-PFCs reveal possible extrasynaptic connectivity. One biological implication of emittance connections that are not PFCs is that the involved neurons

do not necessarily rely on the fixed global anatomy to be functionally connected, and additional structural connections are needed for their functional connectivity to be predicted from anatomy. This is consistent with results from the multiple studies that have demonstrated the presence of extrasynaptic functional signaling between neurons [6, 10, 46, 59, 60]. We tested this interpretation by investigating the PFCs of the motor neuron and interneuron RID which has recently been identified by Randi et al. [59] to generate functional connections that were not predicted from anatomy.

Specifically, we computed the NEP_β of RID at a functional inverse temperature $\beta_f = 1.05\beta_c$ and its emittance network is represented in Figure 2. We found that the emittance connections of RID onto ADLL/R and URXL/R are statistically non-significant ($p = 1$), and its emittance connection onto AWBL/R are very weak ($\leq 10^{-4}$) and statistically non-significant with $p = 1$.

On the other hand, considering an extrasynaptic chemical signaling between neurons as an actual physical connection, we separately added to the graph one edge from RID to URXL and one edge from RID to ADLR. Next, we recomputed the NEP_β of RID within the updated directed graphs and found that (see Supplementary Data 5 and 6) the new neural emittances from RID to URXL and ADLR are PFCs ($p = 0.0082$ and $p = 0.0086$, respectively).

These observations theoretically support the results from [59] that detected functional connections $\text{RID} \rightarrow \text{ADLR}$ and $\text{RID} \rightarrow \text{URXL}$ that are not predicted by the anatomy and that partly rely on chemical extrasynaptic transmissions.

7. Mixed states and pure functional connectomes.

Now observe that any convex combination of NEP_β is a β -KMS state, and, conversely, any KMS state \mathcal{X} can be expressed as a convex combination $\mathcal{X} = \sum_v p_v \mathcal{Z}^{v,\beta}$, where $0 \leq p_v \leq 1$, $\sum_v p_v = 1$ (see Appendix C for details); namely, the KMS state space \mathcal{S}_β is a simplex generated by the NEP_β . The *mixed (KMS) states* are those such that P is not a Dirac distribution. It follows that a mixed β -KMS state \mathcal{X} is completely determined by the column stochastic matrix \mathbf{Z}^β with columns the pure state vectors $\mathcal{Z}^{v,\beta}$ together with a probability distribution $P = (p_v)_v$ on the neurons; that is,

$$\mathcal{X} = \mathbf{Z}^\beta P. \quad (6)$$

Observe that since each column vector $\mathcal{Z}^{v,\beta}$ theoretically measures potential functional connections from a neuron to the other neurons, the whole matrix \mathbf{Z}^β measures all the potential functional connections between each pair of neurons in the connectome. Thus, a mixed β -KMS state \mathcal{X} encodes 1) the potential functional connections between each neuron pair at inverse temperature β , and 2) the expectation value of the upstream connectivity onto each neuron given the probability distribution P on the neurons. It follows that for each β value, \mathbf{Z}^β is a connectivity matrix encoding the 'functional' pathway substrates underlying all connectivity state vectors representing mixed β -KMS states.

Moreover, using the idea of PFCs from the previous paragraph, we get a *pure functional connectivity matrix* at inverse temperature β by restricting \mathbf{Z}^β to its statistically significant values. The resulting matrix is the adjacency matrix of a weighted directed network \mathcal{F}^β whose edges all the PFCs of the connectome at the given β value, and for this reason we call it the '*pure functional connectome*' at inverse temperature β . Specifically, it represents potential functional connections predicted by the topology of the anatomical network.

We investigated \mathcal{F}^β at the functional inverse temperature $\beta_f = 1.05\beta_c$ (see Appendix C and Supplementary Data 3 for the edgelist) and found that it reveals connectivity patterns that coincide with circuitries that have been reported by researchers to be the functional substrates of well studied *C. elegans* complex behaviors such as locomotion and touch-induced movement [17, 73], indicating that our network model provides a theoretical basis for understanding the functional organization of a nervous system.

8. Pure functional connectome reveals the importance of the locomotory circuit.

\mathcal{F}^β has 8932 weighted directed edges, compared to the network \mathcal{K} formed by the structural connectivity of all neurons which has 4927 weighted directed edges (Appendix C for a detailed definition and Supplementary Data 2 for the edgelist). It represents only 11.68% of all the potential functional connections given by the adjacency matrix \mathbf{Z}^β , implying that only about 12% of all neural β -emittance connections are PFCs. This network is schematically represented in Figure 11.

We observed a substantial topological discordance between \mathcal{F}^β and \mathcal{K} . For instance, the motor neuron classes AS, VA, DA, VB, and DB, have the highest in-degree centrality \mathcal{F} , with AS08, DA06, AS07, DA07, VA08, DB05, VA10, DB06, AS09, VA11 being the 10 most central neurons in terms of incoming connections, and specifically AS08, which is ranked 278 in the anatomical network (see Table II), receiving 219 PFCs (see Appendix C). Notably, none of these neurons is among the most in-connected in the structural connectome ($k^{in} = 2$ for AS08 and 7 for DA06) which has the command interneuron classes AVA, AVB, AVE, AVD, and PVC receiving the highest numbers of incoming connections (see Appendix C). Moreover, VA08 has the highest weighted in-degree w^{in} followed by DA06, and DB05 has the largest weighted out-degree w^{out} , while they are poorly anatomically connected. Additionally, some of these neurons are highly ranked in terms of out-degree and weighted out-degree (see Table II). Specifically, DA07 has the second largest number of outgoing connections ($k^{ou} = 64$), compared to its 3 anatomical weighted connections, VB07 has out-degree rank 6 and weighted out-degree rank 7, and DB05 has out-degree rank 9 and weighted out-degree rank 1. Interestingly, PVCL and PVCR are the most functionally in- and out-connected among the command interneurons most of whom have their anatomical status downgraded in the pure functional connectome. Indeed,

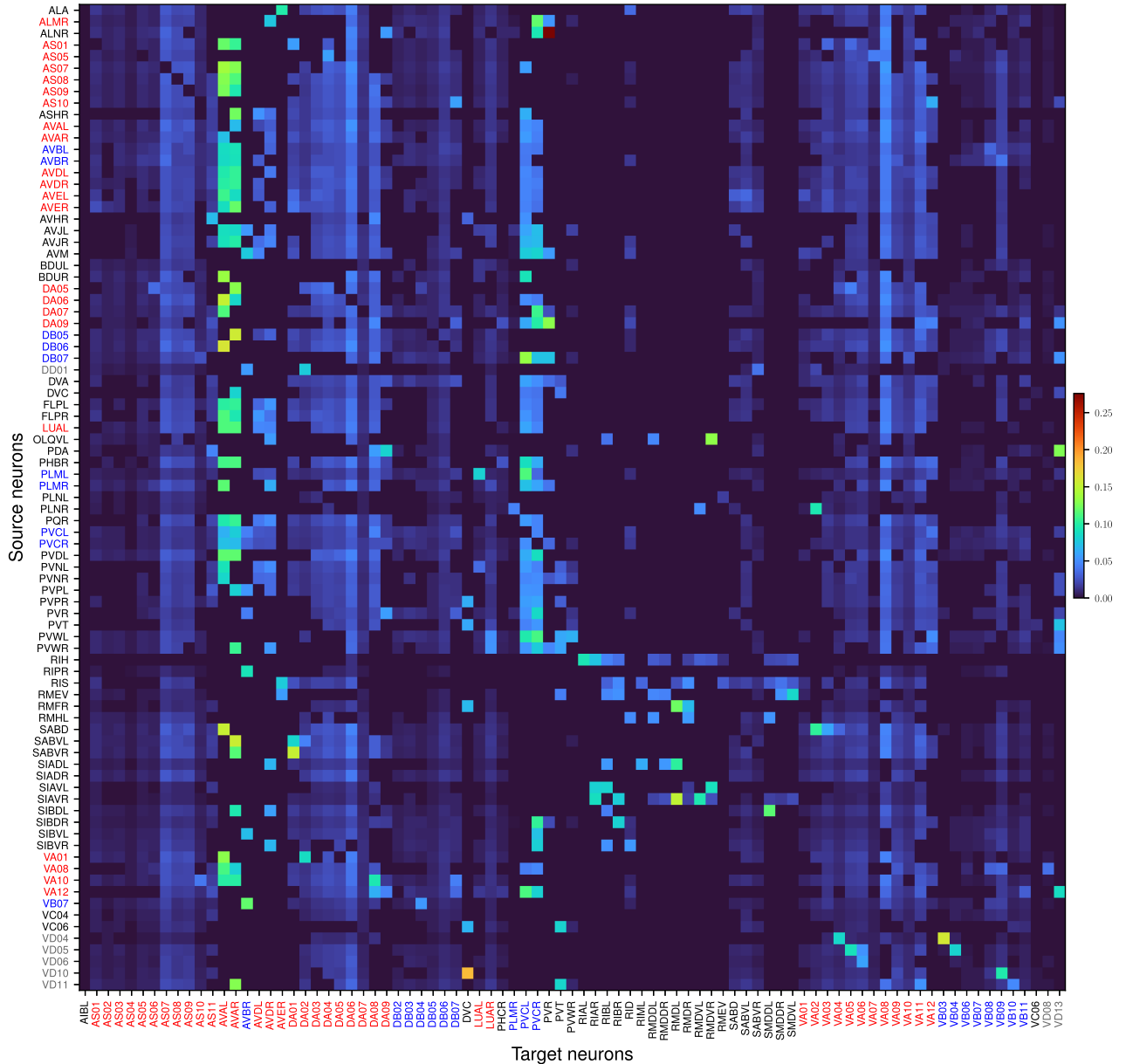


FIG. 3: **Pure functional connectivity matrix.** Representation of part of the adjacency matrix of the pure functional connectome \mathcal{F}^β at $\beta = 1.05\beta_c$. Neurons on the x-axis are the ones with the largest in-degrees in \mathcal{F}^β , and on the y-axis are those with the highest out-degrees.

on the one hand, AVAL, AVAR, PVCL, and PVCR have their respective structural weighted in-degree ranks almost maintained in \mathcal{F}^β , while their weighted out-degree ranks are not, and on the other, PVCL and PVCR have their high structural out-degree ranks almost maintained in \mathcal{F}^β while their weighted out-degree ranks are not.

Overall, as Fig. 3 shows, the command interneurons globally have higher weighted degrees than the motor A and B cell types, albeit with lesser connections. Thus, both groups constitute the most central neurons of the pure functional connectome. In other words, show that the sets of ventral cord motor neuron classes AS, A, and B,

are well positioned in the nervous system to be the target of most information flow pathways within the connectome, and the command interneuron classes AVA, AVB, AVD, AVE, while PVC send and receive the most intense ones. This theoretical result is consistent with experimental studies that have described the central role played by these neurons locomotion [17, 50, 73], which has been shown to be the core of all the *C. elegans* functions and behaviors [12, 54].

9. Mechanoreceptor neurons have higher functional out-degree. Additionally, we found that the posterior mechanoreceptor neuron [29] PLML is the most cen-

In-degree ranking					Out-degree ranking				
Neuron	\mathcal{F}^β		\mathcal{K}		Neuron	\mathcal{F}^β		\mathcal{K}	
	k^{in}	w^{in}	k^{in}	w^{in}		k^{out}	w^{out}	k^{out}	w^{out}
AS08	1	10	278	278	PLML	1	259	272	158
DA06	2	2	248	248	DA07	2	273	274	146
AS07	3	6	269	270	PVCR	3	113	5	163
DA07	4	44	256	275	SIBDR	4	52	248	74
VA08	5	1	193	115	PVCL	5	185	4	115
DB05	6	72	236	274	VB07	6	7	261	200
VA10	7	30	257	259	SABVL	7	197	269	198
DB06	8	32	249	273	SIBDL	8	266	224	209
AS09	9	15	270	256	DB05	9	1	276	150
VA11	10	8	183	179	SIBVL	10	137	176	208
DA04	11	11	142	202	AS08	11	183	279	143
VA06	12	21	181	217	DB06	12	228	275	147
AS06	13	94	223	255	AS10	13	196	253	83
AS05	14	87	208	257	SIAVR	14	216	250	187
DA05	15	16	92	134	VA10	15	231	255	196
VA07	16	85	222	216	SIADR	16	136	178	31
AS04	17	178	235	272	SIBVR	17	138	181	57
AS10	18	105	179	234	VD11	18	257	244	109
VA05	19	35	154	162	VD05	19	84	217	216
VA09	20	24	182	164	AVAR	20	18	1	268
DA08	21	9	82	85	AVAL	21	2	2	114
AS02	22	147	207	254	SABVR	22	34	268	108
DA03	23	23	98	143	ALA	23	17	179	55
VB06	24	173	226	263	AS09	24	88	273	144
VA04	25	79	156	168	DB07	25	112	201	191
VB09	26	38	211	181	PVR	26	246	8	117
AS03	27	130	192	253	ALMR	27	247	183	121
AS01	28	101	178	243	SABD	28	33	259	195
LUAR	29	84	170	204	AVBR	29	4	6	26
VA03	30	62	153	136	DVA	30	129	3	278
SABVR	31	144	210	242	VC04	31	169	245	203
PVCL	32	5	8	8	VD08	32	93	271	156
VD08	33	109	273	123	VD06	33	175	238	82
DA02	34	76	66	118	AS07	34	3	267	190
VB11	35	127	194	245	DA06	35	20	254	111
VB07	36	194	227	262	AVBL	36	189	7	13
SABVL	37	97	184	214	SIADL	37	51	235	212
DA01	38	57	155	62	PVWL	38	254	222	86
VB10	39	177	239	209	AVDR	39	5	9	7
PHCR	40	185	212	231	PVNR	40	269	11	101
AS11	41	74	74	147	VD10	41	256	262	153
PVCR	42	7	9	6	AVDL	42	19	18	164
AVAR	43	4	2	2	DVC	43	58	29	51
AVAL	44	3	1	1	BDUL	44	16	173	29

TABLE II: **Degree and weighted degree centrality.** Ranking of neurons with respect to the in- and out-degree (k^{in} and k^{out}) and the weighted in- and out-degree (w^{in} and w^{out}) of the pure functional connectome \mathcal{F}^β and the weighted structural network \mathcal{K} .

tral in number of outgoing connections in \mathcal{F}^β ($k^{out} = 66$), and the anterior mechanoreceptor ALMR is among the 30 most out-connected with $k^{out} = 54$ in \mathcal{F}^β (ranked 27 in Table II). By comparison, both neurons have very low out-degrees of respectively 4 and 12 and low ranks of 272 and 183 in the structural network \mathcal{K} , and both neurons have low ranks in terms of weighted out-degree (259 and 247, respectively). More generally, we observed

that many mechanoreceptor neurons [29, 40, 74], including ALA, ASHR, AVM, DVA, FLPL/R, OLQVL, etc., are among the most out-connected in \mathcal{F}^β .

10. Integration capacity of neurons. We now consider a particular mixed KMS state defined as follows. Letting P in (6) be the uniform distribution $p_v = 1/N$ on V , the resulting mixed KMS state $\langle \mathcal{Z}^{v,\beta} \rangle = \frac{1}{N} \sum \mathcal{Z}^{v,\beta}$ is the mean NEP_β , and the receptance of a neuron u in

this state is the average neural emittance to u at inverse temperature β .

The mixed state $\langle \mathcal{Z}^{v,\beta} \rangle$ encodes all the possible information pathways upstream of every neuron, which might involve feedback pathways. Thus, comparing two neurons according to their respective receptance in this state can be biased if, for example, most incoming paths to one neuron consists of feedback loops, while the other one mostly receives pathways that do not communicate to each other through cycles. In order to quantify the extent to which a neuron u 'integrates' independent pathways, we introduce the following measure that we call the *integration capacity* $0 \leq \mathbf{IC} \leq 1$ at inverse temperature β :

$$\mathbf{IC}_u(\beta) = \frac{1}{N-1} \left(N \langle \mathcal{Z}^{v,\beta} \rangle_u - \mathcal{Z}_u^{u,\beta} \right). \quad (7)$$

Specifically, it is the 'expected' relative total weight of all the possible PFC onto the neuron excluding its neural self-emittance at inverse temperature β . A high \mathbf{IC} value at a given temperature means a high likelihood of receiving any information flowing across the network, which reflects two topological features of the neuron: 1) it is the target of a relatively large number of independent flow pathways of certain lengths; in other words, a high capacity for the neuron to integrate information flows coming from many different neurons that do not belong to the same cycles; in particular, the \mathbf{IC} of a highly connected neuron with nearly no closed paths will be close to 1, whereas an equally connected neuron whose almost all incoming paths are cycles will have an \mathbf{IC} close to 0; and 2) it has substantial redundancies among its incoming pathways; in other words, the neuron is well-situated in the connectome to receive inputs from multiple neurons via a number of parallel pathways of certain range.

In one sense, neurons whose \mathbf{IC} is high at small temperature values but low at larger temperature values are structurally positioned to mediate relatively short-range communications, making them '*local integrators*' [52], whereas those with high \mathbf{IC} at higher temperatures are '*global integrators*' capable of mediating multiple long-range incoming communications. To better understand the functional properties of the \mathbf{IC} , we analyzed its variation with respect to temperature to classify neurons based on the behavior of their \mathbf{IC} function. We observed four main neuron groups showing different integration behaviors (see Table III for the complete classification) schematically illustrated by Fig. 4 and characterized as follows.

a. Group 1 - For these neurons, \mathbf{IC} increases indefinitely with temperature, following an exponential law (Fig. 4a). This group contains the touch receptor neurons ALMR, AVM, PLML/R, and PVM [17, 29], as well as all the neurons known to be involved in the locomotion functional circuit [50, 71, 73]; namely, the command interneuron classes AVA, AVB, AVD, AVE, and PVC, and the motor neuron classes A, B, and D.

b. Group 2 - \mathbf{IC} increases with temperature and 'saturates' at a maximum value within an inverse temperature

interval I_f between $1.02\beta_c$ and $1.07\beta_c$, before dropping to zero around the critical temperature (Fig. 4b); this implies that redundancy among upstream pathways of these neurons becomes rare above certain path length. Neurons belonging to this group include the chemosensory [4] neuron classes ADL, ADF, ASE, ASG, ASI, ASJ, ASK, AWA, AWB, and URX, as well as all the neuron classes AIA, AIB, AFD, AWC, AIY, AIZ, and RIA which are known to mediate the worm's *thermotaxis* behavior [43, 44, 47, 49].

c. Groups 3 and 4 - For a small number of neurons including ADAL/R, HSNR, PHAL/R, PHBR, etc., \mathbf{IC} increases until it reaches a near plateau within the same interval $I_f = [1.02\beta_c, 1.07\beta_c]$, followed by an inflection point with a positive (*group 3*) or negative (*group 4*) slope, before rising again around the critical temperature (Figs. 4c & d). This implies that for these neurons, redundancy fluctuates among upstream pathways of above certain path length.

11. Asymmetrical integration. Some neuron classes show asymmetry in their integration capacity. For instance, the touch receptor neuron ALMR is in *group 1* while its sister cell ALML belongs to *group 2* (see III). The polymodal amphid sensory neuron class ASH, which has been shown [28, 33, 40] to have a multisensory integration function, has its right cell ASHR in *group 1* and left one ASHL in *group 2*. While PHAL and PHAR are both in *group 3*, PHBL belongs to *group 1* and its sister cell PHBR is in *group 3*. This indicates that among the phasmid neuron classes PHA and PHB, which have been shown [33, 36] to belong to an antagonistic functional circuit that integrates sensory responses from the amphids ASH and ASK to mediate *chemo-repulsion* behavior, PHBR is structurally well positioned to have greater long-range integration function.

12. \mathbf{IC} predicts response of AIY in AFD- or AWC-ablated animals. As a direct application of the \mathbf{IC} measure, we theoretically reproduced an experimental study by Kano et al. [39] that has shown that the thermosensory neuron class AWC regulates the information processing in the AFD-AWC-AIY circuit [43, 44], which is part of the functional circuit mediating the *C. elegans*' *thermotaxis*' behavior [47, 49].

Specifically, we study the \mathbf{IC} variation of AIYL and AIYR within the connectome of wild-type (WT) animal and within that of x -ablated animal, where x is either one or both of the neurons in the AFD or AWC class. We shall note that in [39], the authors did not investigate the individual neurons AFDL, AFDR, AWCL, AWCR, AIYL, and AIYR separately, but only considered the corresponding neuron classes. Here, our model being based on individual neurons, we can theoretically evaluate the extent to which removing each one of them impacts the information flow and integration capacity of the others. Indeed, to theoretically represent the ablation of a neuron, we just remove from the graph all the anatomical connections going in and out of it, in order to keep the same dimension for the resulting connectivity state vec-

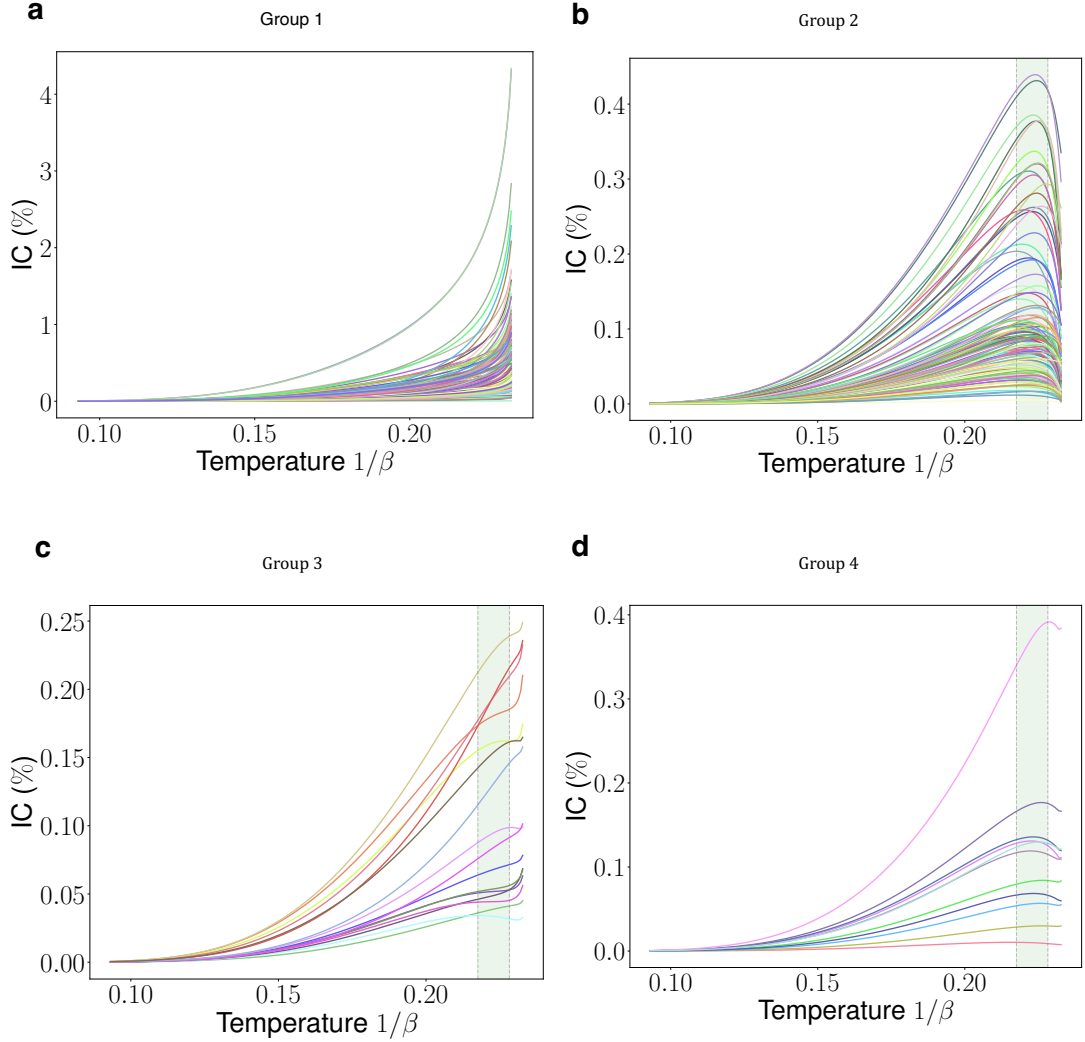


FIG. 4: **Integration capacity (IC)**. Graphic representations of the IC of all neurons as a function of temperature. The behavior of the integration capacity function segregates the connectome into four groups of neurons, each characterized by the global shapes of the IC curves as represented by a, b, c, and d, respectively. The shaded area shows the *optimal temperature interval* within which the IC function reaches either a maximum for group 2 neurons or a near plateau for group 3 and 4.

tors. We then compared investigated the IC of AIYL and AIYR before and after by comparing their variations using a Kolmogorov–Smirnov statistical test. The results of this analysis are graphically presented in 6, summarized by Figure 5, and detailed as follows:

- In wild-type animal connectome, there is an IC asymmetry between AIYL and AIYR; namely, the KS-test shows that the IC of AIYR is significantly higher than that of AIYL ($p = 10^{-8}$).
- In AFDL- or AWCL-ablated animal connectome (Figs. 6a & d), the IC of AIYL significantly decreases ($p < 10^{-14}$), while the IC of AIYR remains the same as for wild-type connectome ($p \simeq 0.93$).
- Ablation of AFDR (Fig. 6b) significantly decreases the IC of AIYR ($p = 3.10^{-23}$) but does not affect

AIYL ($p = 0.2$), and ablation of AWCR (Fig. 6e) significantly decreases the IC of both AIYL ($p = 10^{-7}$) and AIYR ($p = 10^{-12}$) while significantly reducing the IC asymmetry between AIYL and AIYR ($p = 0.002$).

- In the connectome of animals with both AFDL and AFDR ablated (Fig. 6c), the IC significantly decreases in AIYL ($p = 2.10^{-16}$) and AIYR ($p = 8.10^{-24}$), and both AIYL and AIYR have the same IC ($p = 0.12$).
- Ablation of both AWCL and AWCR (Fig. 6f) not only significantly decreases the IC of both AIYL ($p = 10^{-23}$) and AIYR ($p = 7.10^{-13}$) but also increases the IC asymmetry between AIYR and AIYL ($p = 3.10^{-18}$).

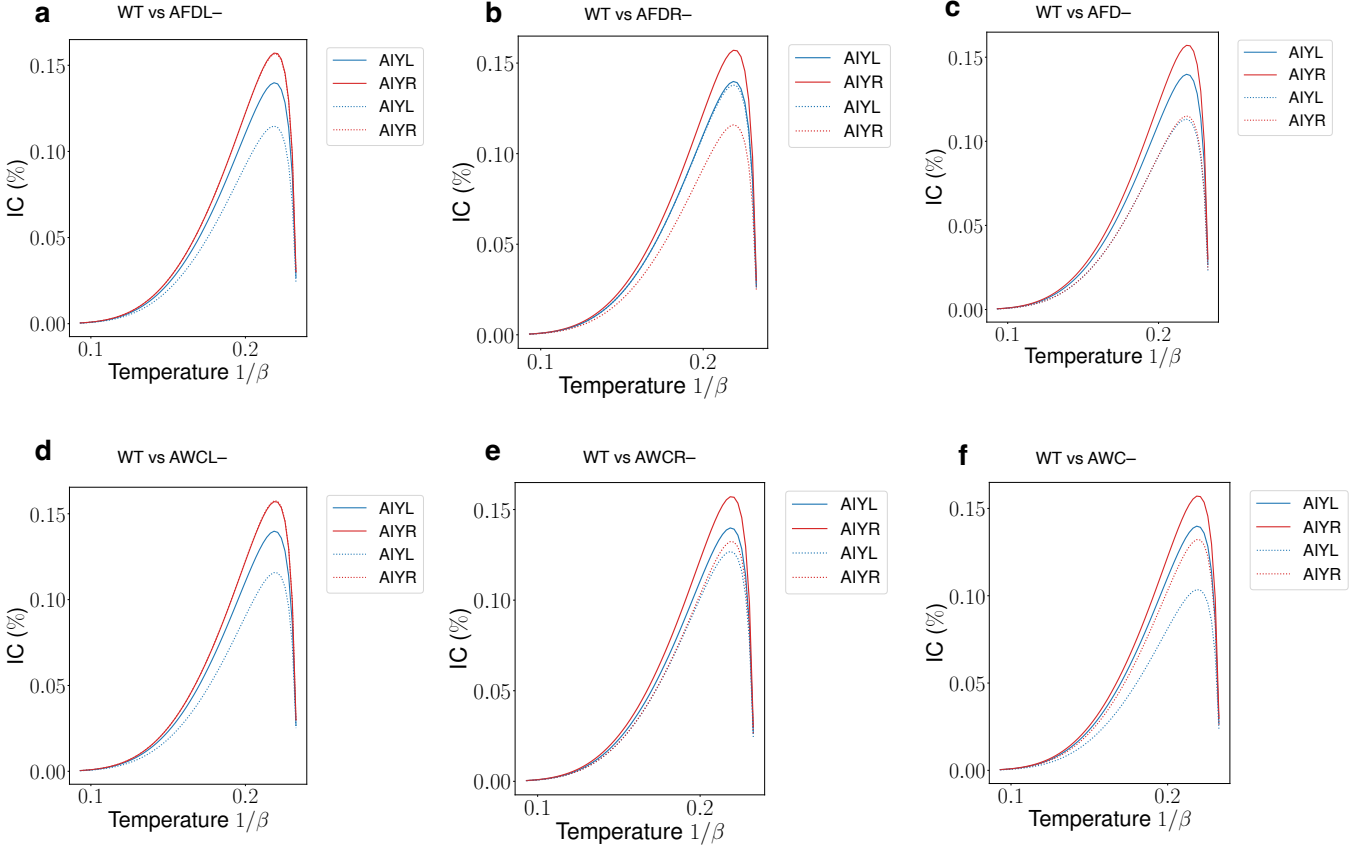


FIG. 6: **Change of the IC of AIY.** Comparison of the IC variation of AIYL and AIYR between the connectome of wild-type (WT) animals and the connectome of animals in which either one or both neurons in the AFD or AWC class are ablated. Continuous lines represent WT, and dashed lines represent IC when an individual neuron or a neuron class is ablated. Comparison is made using the two-sample Kolmogorov-Smirnov statistical test. In WT, AIYL and AIYR are asymmetrical in terms of their IC, with AIYR's IC significantly higher than that of AIYL ($p = 10^{-8}$). a: The IC is compared between WT and AFDL-ablated: only AIYL has its IC significantly impacted (decreased). b: WT compared to AFDR-ablated: only AIYR has IC impacted. c: WT compared to both AFDL and AFDR ablated: both AIYL and AIYR have lower IC while their IC asymmetry is eliminated. d: WT compared to AWCL-ablated: only AIYL's IC decreases. e: WT compared to AWCR-ablated: both AIYL and AIYR have lower IC and their asymmetry is significantly reduced. f: WT compared to both AWCL and AWCR ablated: both AIYL and AIYR have lower IC, while the IC asymmetry significantly increases.

as the one defined by the neuropeptidergic signaling.

Furthermore, our results from the integration capacity analysis and simulations of individual cell ablation within the thermotaxis neuronal circuit theoretically explain the in vivo studies of Kano et al. [39] and reveal the functional asymmetry of the thermosensory neuron class AWC, which regulates information processing in the AFD-AWC-AIY sub-circuit, as well as the interneuron class AIY, paving the way for further investigations into the functional differences among neurons of the same class and how the activity of one neuron influences another.

Finally, although we used the *C. elegans* connectome to illustrate our work, the formalism developed here is broad and can be applied to general directed complex networks to understand their functional properties.

METHODS

The *C. elegans* somatic connectome. We have merged two datasets of the somatic connectome of the hermaphrodite worm *C. elegans* that are publicly available on the WormAtlas [2]: the first dataset, *Data1*, is from Varshney et al. [71], and the second one, *Data2*, is from the recently published serial electron microscopy reconstructions by Cook et al. [19]. Specifically, we have kept all synaptic connections from *Data1* (279 connected neurons and 8171 chemical and electrical synapses), to which we have added all synaptic connections in *Data2* that were not originally in *Data1* (3900 additional connections). The resulting connectome consists of 280 connected neurons and 12071 synaptic connections. Note that in the old version (*Data1*), VC06 had no connections, while it is connected in the revised connectome.

Computing the structure-function divergence and the mean total receptance. To calculate $\text{sfd}(v, \beta)$ for a neuron, we have used the distributions $\underline{\mathcal{K}}^v$ and $\underline{\mathcal{Z}}^{v,\beta}$ instead of \mathcal{K}^v and $\mathcal{Z}^{v,\beta}$, respectively, where $\underline{\mathcal{K}}_v^v = 0$, $\underline{\mathcal{Z}}_v^{v,\beta} = 0$, and for $u \neq v$, $\underline{\mathcal{K}}_u^v = \mathcal{K}_u^v / \sum_{w \neq v} \mathcal{K}_w^v$ if $\mathcal{K}_u^v > 0$, and $\underline{\mathcal{Z}}_u^{v,\beta} = \mathcal{Z}_u^{v,\beta} / \sum_{w \neq v} \mathcal{Z}_w^{v,\beta}$, provided $\mathcal{Z}_u^{v,\beta} > 0$.

Mean total receptance. The mean total receptance at inverse temperature β is given by the formula

$$\frac{\sum_v \sum_{u \neq v} \underline{\mathcal{Z}}_u^{v,\beta}}{N(N-1)}. \quad (8)$$

Statistical significance of neural emittance. In order to know the extent to which a given neural β -

emittance is statistically significant, we used a bootstrapping technique consisting of generating 5000 random directed graphs with the same degree sequence as the graph G representing the connectome, and computing the neural emittance of the same neuron in each generated graph at the same inverse temperature β . The neural emittance is then statistically significant if it occurs with the same or larger value in less than 5% of the time ($p < 0.05$).

DATA AND CODE AVAILABILITY

The code written for this work and the data generated are available in the public domain at <https://github.com/elkMm/KMSnet>.

-
- [1] L. F. Abbott, D. D. Bock, E. M. Callaway, W. Denk, C. Dulac, A. L. Fairhall, I. Fiete, K. M. Harris, M. Helmstaedter, V. Jain, N. Kasthuri, Y. LeCun, J. W. Lichtman, P. B. Littlewood, L. Luo, J. H. Maunsell, R. C. Reid, B. R. Rosen, G. M. Rubin, T. J. Sejnowski, H. S. Seung, K. Svoboda, D. W. Tank, D. Tsao, and D. C. Van Essen. The mind of a mouse. *Cell*, 182(6):1372–1376.
- [2] Z. Altun, L. Herndon, C. Wolkow, C. Crocker, R. Lints, and D. Hall. WormAtlas. <https://www.wormatlas.org> [Accessed: 20.03.2024].
- [3] A. an Huef, M. Laca, I. Raeburn, and A. Sims. KMS states on the C^* -algebras of finite graphs. *Journal of Mathematical Analysis and Applications*, 405, 05 2012.
- [4] C. Bargmann. Chemosensation in *c. elegans* (October 25, 2006). *WormBook*, ed. The *C. elegans* Research Community, WormBook, doi/10.1895/wormbook.1.123.1, <http://www.wormbook.org>.
- [5] C. I. Bargmann and E. Marder. From the connectome to brain function. *Nature Methods*, 10(6):483–490, 2013.
- [6] A. Barrios, R. Ghosh, C. Fang, S. W. Emmons, and M. M. Barr. Pdf-1 neuropeptide signaling modulates a neural circuit for mate-searching behavior in *c. elegans*. *Nature Neuroscience*, 15(12):1675–1682.
- [7] T. Bates, D. Pask, I. Raeburn, and W. Szymanski. The C^* -algebras of row-finite graphs. *New York Journal of Mathematics*, 6:307–324, 01 2000.
- [8] J. M. Bekkers. Synaptic transmission: Functional autapses in the cortex. *Current Biology*, 13(11):R433–R435, 2003.
- [9] P. Bellec, V. Perlbarg, S. Jbabdi, M. Péligrini-Issac, J.-L. Anton, J. Doyon, and H. Benali. Identification of large-scale networks in the brain using fmri. *NeuroImage*, 29(4):1231–1243.
- [10] B. Bentley, R. Branicky, C. L. Barnes, Y. L. Chew, E. Yemini, E. T. Bullmore, P. E. Vértes, and W. R. Schafer. The multilayer connectome of *caenorhabditis elegans*. *PLoS Computational Biology*, 12(12):1–31, 12 2016.
- [11] R. G. Bettinardi, G. Deco, V. M. Karlaftis, T. J. Van Hartevelt, H. M. Fernandes, Z. Kourtzi, M. L. Kringelbach, and G. Zamora-López. How structure sculpts function: Unveiling the contribution of anatomical connectivity to the brain’s spontaneous correlation structure. *Chaos: An Interdisciplinary Journal of Nonlinear Science*, 27(4).
- [12] M. d. Bono and A. Villu Maricq. Neuronal substrates of complex behaviors in *c. elegans*. *Annual Review of Neuroscience*, 28(1):451–501.
- [13] J. B. Bost and A. Connes. Hecke algebras, type III factors and phase transitions with spontaneous symmetry breaking in number theory. *Selecta Mathematica*, 1(3):411–457, 1995.
- [14] O. Bratteli and D. W. Robinson. *Operator Algebras and Quantum Statistical Mechanics II. Equilibrium States Models in Quantum Statistical Mechanics*, volume 62 of *Theoretical and Mathematical Physics*. Springer Berlin, Heidelberg, 1982.
- [15] T. Bühler and D. Salamon. *Functional Analysis*. Graduate studies in mathematics. American Mathematical Society, 2018.
- [16] E. Bullmore and O. Sporns. The economy of brain network organization. *Nature Reviews Neuroscience*, 13(5):336–349, 2012.
- [17] M. Chalfie, J. E. Sulston, J. G. White, E. Southgate, J. N. Thomson, and S. Brenner. The neural circuit for touch sensitivity in *caenorhabditis elegans*. *J Neurosci*, 5(4):956–964, Apr 1985.
- [18] A. Connes. *Noncommutative Geometry*. Elsevier Science, 1995.
- [19] S. Cook, T. Jarrell, C. Brittin, Y. Wang, A. Bloniarz, M. Yakovlev, K. Nguyen, L. Tang, E. Bayer, J. Duerr, H. Bülow, O. Hobert, D. Hall, and S. Emmons. Whole-animal connectomes of both *caenorhabditis elegans* sexes. *Nature*, 571:63, 07 2019.
- [20] J. J. R. Cuntz and W. Krieger. A class of C^* -algebras and topological markov chains. *Inventiones mathematicae*, 56:251–268, 1980.
- [21] J. DeFelipe. From the connectome to the synaptome: An epic love story. *Science*, 330(6008):1198–1201, 2010.
- [22] R. S. Desikan, F. Ségonne, B. Fischl, B. T. Quinn, B. C. Dickerson, D. Blacker, R. L. Buckner, A. M. Dale, R. P. Maguire, B. T. Hyman, M. S. Albert, and R. J. Killiany. An automated labeling system for subdividing the human cerebral cortex on mri scans into gyral based regions of interest. *NeuroImage*, 31(3):968–980.
- [23] J. Dixmier. *C^* -algebras*. North-Holland mathematical library. North-Holland, 1982.

- [24] J. Doyon and H. Benali. Reorganization and plasticity in the adult brain during learning of motor skills. *Current Opinion in Neurobiology*, 15(2):161–167.
- [25] S. W. Emmons. The mood of a worm. *Science*, 338(6106):475–476, 2012.
- [26] E. Estrada and N. Hatano. Communicability in complex networks. *Phys. Rev. E*, 77:036111, Mar 2008.
- [27] K. Friston, C. Frith, P. Liddle, and R. Frackowiak. Functional connectivity: the principal-component analysis of large (pet) data sets. *Journal of Cerebral Blood Flow & Metabolism*, 13(1):5–14, 1993.
- [28] D. D. Ghosh, M. N. Nitabach, Y. Zhang, and G. Harris. Multisensory integration in *c. elegans*. *Current Opinion in Neurobiology*, 43:110–118.
- [29] M. B. Goodman. Mechanosensation (January 06, 2006). *WormBook*, ed. The *C. elegans* Research Community, WormBook, doi/10.1895/wormbook.1.62.1 <http://www.wormbook.org>.
- [30] R. Haag, N. M. Hugenholtz, and M. Winnink. On the equilibrium states in quantum statistical mechanics. *Communications in Mathematical Physics*, 5(3):215–236, June 1967.
- [31] B. C. Hall. *Quantum Theory for Mathematicians*. Springer New York.
- [32] L. H. Hartwell, J. J. Hopfield, S. Leibler, and A. W. Murray. From molecular to modular cell biology. *Nature*, 402(6761):C47–C52, 1999.
- [33] M. A. Hilliard, C. I. Bargmann, and P. Bazzicalupo. *C. elegans* responds to chemical repellents by integrating sensory inputs from the head and the tail. *Current Biology*, 12(9):730–734, 2002.
- [34] N. M. Hugenholtz. *The how, why and wherefore of C^* -algebras in statistical mechanics*, pages 641–647. Springer Berlin Heidelberg, Berlin, Heidelberg, 1972.
- [35] V. Jakšić and C. A. Pillet. Mathematical theory of non-equilibrium quantum statistical mechanics. *Journal of Statistical Physics*, 108(5):787–829, 2002.
- [36] T. A. Jarrell, Y. Wang, A. E. Bloniarz, C. A. Brittin, M. Xu, J. N. Thomson, D. G. Albertson, D. H. Hall, and S. W. Emmons. The Connectome of a Decision-Making Neural Network. *Science*, 337(6093):437–444, 2012.
- [37] R. Jozsa. Fidelity for Mixed Quantum States. *Journal of Modern Optics*, 41:2315–2323, 1994.
- [38] T. Kajiwara and Y. Watatani. KMS states on finite-graph C^* -algebras. *Kyushu Journal of Mathematics*, 67, 07 2010.
- [39] A. Kano, H. J. Matsuyama, S. Nakano, and I. Mori. AWC thermosensory neuron interferes with information processing in a compact circuit regulating temperature-evoked posture dynamics in the nematode *Caenorhabditis elegans*. *Neuroscience Research*, 188:10–27, 2023.
- [40] J. M. Kaplan and H. R. Horvitz. A dual mechanosensory and chemosensory neuron in *Caenorhabditis elegans*. *Proceedings of the National Academy of Sciences of the United States of America*, 90:2227 – 2231, 1993.
- [41] L. Katz. A new status index derived from sociometric analysis. *Psychometrika*, 18(1):39–43, 1953.
- [42] M. Kivelä, A. Arenas, M. Barthélemy, J. P. Gleeson, Y. Moreno, and M. A. Porter. Multilayer networks. *Journal of complex networks*, 2(3):203–271, 2014.
- [43] A. Kuhara, N. Ohnishi, T. Shimowada, and I. Mori. Neural coding in a single sensory neuron controlling opposite seeking behaviours in *Caenorhabditis elegans*. *Nature Communications*, 2(1):355, 2011.
- [44] A. Kuhara, M. Okumura, T. Kimata, Y. Tanizawa, R. Takano, K. D. Kimura, H. Inada, K. Matsumoto, and I. Mori. Temperature sensing by an olfactory neuron in a circuit controlling behavior of *c. elegans*. *Science*, 320(5877):803–807, 2008.
- [45] A. Kumjian, D. Pask, and I. Raeburn. Cuntz-Krieger algebras of directed graphs. *Pacific Journal of Mathematics*, 184, 09 1998.
- [46] M. A. Lim, J. Chitturi, V. Laskova, J. Meng, D. Findels, A. Wiekenberg, B. Mulcahy, L. Luo, Y. Li, Y. Lu, W. Hung, Y. Qu, C.-Y. Ho, D. Holmyard, N. Ji, R. McWhirter, A. D. Samuel, D. M. Miller, R. Schnabel, J. A. Calarco, and M. Zhen. Neuroendocrine modulation sustains the *C. elegans* forward motor state. *eLife*, 5.
- [47] X. Ma and Y. Shen. Structural basis for degeneracy among thermosensory neurons in *Caenorhabditis elegans*. *Journal of Neuroscience*, 32(1):1–3, 2012.
- [48] A. Messé, D. Rudrauf, H. Benali, and G. Marrelec. Relating structure and function in the human brain: Relative contributions of anatomy, stationary dynamics, and non-stationarities. *PLoS computational biology*, 10:e1003530, 03 2014.
- [49] I. Mori, H. Sasakura, and A. Kuhara. Worm thermotaxis: a model system for analyzing thermosensation and neural plasticity. *Current Opinion in Neurobiology*, 17(6):712–719, 2007. Motor systems / Neurobiology of behaviour.
- [50] F. Morone and H. A. Makse. Symmetry group factorization reveals the structure-function relation in the neural connectome of *Caenorhabditis elegans*. *Nature Communications*, 10(1):4961, 2019.
- [51] E. M. Moutouou, O. B. K. Ali, and H. Benali. Topology and spectral interconnectivities of higher-order multilayer networks. *Frontiers in Complex Systems*, 1, 2023.
- [52] H.-J. Park and K. Friston. Structural and functional brain networks: From connections to cognition. *Science*, 342(6158):1238411, 2013.
- [53] A. E. Pereda. Electrical synapses and their functional interactions with chemical synapses. *Nature Reviews Neuroscience*, 15(4):250–263, 2014.
- [54] B. Piggott, J. Liu, Z. Feng, S. Wescott, and X. Xu. The neural circuits and synaptic mechanisms underlying motor initiation in *c. elegans*. *Cell*, 147(4):922–933.
- [55] M. Porta-de-la Riva, A. C. Gonzalez, N. Sanfeliu-Cerdán, S. Karimi, N. Malaiwong, A. Pidde, L.-F. Morales-Curiel, P. Fernandez, S. González-Bolívar, C. Hurth, and M. Krieg. Neural engineering with photons as synaptic transmitters. *Nature Methods*, 20(5):761–769.
- [56] F. Pulvermüller, M. Garagnani, and T. Wennekers. Thinking in circuits: toward neurobiological explanation in cognitive neuroscience. *Biological Cybernetics*, 108(5):573–593.
- [57] I. Rabinowitch, D. A. Colón-Ramos, and M. Krieg. Understanding neural circuit function through synaptic engineering. *Nature Reviews Neuroscience*, 25(2):131–139.
- [58] I. Raeburn. *Graph Algebras*. Regional conference series in mathematics. Conference Board of the Mathematical Sciences, 2005.
- [59] F. Randi, A. K. Sharma, S. Dvali, and A. M. Leifer. Neural signal propagation atlas of *Caenorhabditis elegans*. *Nature*, 623(7986):406–414, 2023.
- [60] L. Ripoll-Sánchez, J. Watterne, H. Sun, R. Fernandez, S. R. Taylor, A. Weinreb, B. L. Bentley, M. Hammarlund, D. M. Miller, O. Hobert, I. Beets, P. E. Vértes, and W. R. Schafer. The neuropeptidergic connectome of *c. elegans*.

- Neuron*, 111(22):3570–3589.e5, 2023.
- [61] D. N. Scott and M. J. Frank. Adaptive control of synaptic plasticity integrates micro- and macroscopic network function. *Neuropsychopharmacology*, 48(1):121–144.
- [62] A. Shapson-Coe, M. Januszewski, D. R. Berger, A. Pope, Y. Wu, T. Blakely, R. L. Schalek, P. H. Li, S. Wang, J. Maitin-Shepard, N. Karlupia, S. Dorckenwald, E. Sjostedt, L. Leavitt, D. Lee, J. Troidl, F. Collman, L. Bailey, A. Fitzmaurice, R. Kar, B. Field, H. Wu, J. Wagner-Carena, D. Aley, J. Lau, Z. Lin, D. Wei, H. Pfister, A. Peleg, V. Jain, and J. W. Lichtman. A petavoxel fragment of human cerebral cortex reconstructed at nanoscale resolution. *Science*, 384(6696).
- [63] M. Skuhersky, T. Wu, E. Yemini, A. Nejatbakhsh, E. Boyden, and M. Tegmark. Toward a more accurate 3d atlas of *c. elegans* neurons. *BMC Bioinformatics*, 23(1):195, 2022.
- [64] O. Sporns. Graph theory methods: applications in brain networks. 20(2):111–121.
- [65] O. Sporns. The human connectome: A complex network. *Annals of the New York Academy of Sciences*, 1224:109–25, 04 2011.
- [66] O. Sporns, G. Tononi, and R. Kötter. The human connectome: A structural description of the human brain. *PLoS Computational Biology*, 1(4):null, 09 2005.
- [67] P. Stein. A note on the volume of a simplex. *The American Mathematical Monthly*, 73(3):299–301, 1966.
- [68] G. Tamás, E. H. Buhl, and P. Somogyi. Massive autaptic self-innervation of GABAergic neurons in cat visual cortex. *Journal of Neuroscience*, 17(16):6352–6364, 1997.
- [69] A. Uhlmann. The “transition probability” in the state space of a $*$ -algebra. *Reports on Mathematical Physics*, 9(2):273–279, 1976.
- [70] M. P. van den Heuvel, S. C. de Lange, A. Zalesky, C. Seguin, B. T. Yeo, and R. Schmidt. Proportional thresholding in resting-state fmri functional connectivity networks and consequences for patient-control connectome studies: Issues and recommendations. *NeuroImage*, 152:437–449.
- [71] L. R. Varshney, B. L. Chen, E. Paniagua, D. H. Hall, and D. B. Chklovskii. Structural properties of the *caenorhabditis elegans* neuronal network. *PLoS Computational Biology*, 7(2):1–21, 02 2011.
- [72] C. Veraszto, S. Jasek, M. Gühmann, L. A. Bezares-Calderón, E. A. Williams, R. Shahidi, and G. Jékely. Whole-body connectome of a segmented annelid larva. *eLife*.
- [73] J. G. White, E. Southgate, J. N. Thomson, S. Brenner, et al. The structure of the nervous system of the nematode *caenorhabditis elegans*. *Philos Trans R Soc Lond B Biol Sci*, 314(1165):1–340, 1986.
- [74] S. Wicks and C. Rankin. Integration of mechanosensory stimuli in *caenorhabditis elegans*. *The Journal of Neuroscience*, 15(3):2434–2444.
- [75] M. Winding, B. D. Pedigo, C. L. Barnes, H. G. Patsolic, Y. Park, T. Kazimiers, A. Fushiki, I. V. Andrade, A. Khandelwal, J. Valdes-Aleman, F. Li, N. Randel, E. Barsotti, A. Correia, R. D. Fetter, V. Hartenstein, C. E. Priebe, J. T. Vogelstein, A. Cardona, and M. Zlatić. The connectome of an insect brain. *Science*, 379(6636):eadd9330, 2023.
- [76] D. Witvliet, B. Mulcahy, J. K. Mitchell, Y. Meirovitch, D. R. Berger, Y. Wu, Y. Liu, W. X. Koh, R. Parvathala, D. Holmyard, R. L. Schalek, N. Shavit, A. D. Chisholm, J. W. Lichtman, A. D. T. Samuel, and M. Zhen. Connectomes across development reveal principles of brain maturation. *Nature*, 596(7871):257–261.
- [77] S. L. Woronowicz. On the existence of KMS states. *Letters in Mathematical Physics*, 10:29–31, 1985.
- [78] G. Yan, P. E. Vértes, E. K. Towilson, Y. L. Chew, D. S. Walker, W. R. Schafer, and A.-L. Barabási. Network control principles predict neuron function in the *caenorhabditis elegans* connectome. *Nature*, 550(7677):519–523.
- [79] M. Yu, O. Sporns, and A. J. Saykin. The human connectome in alzheimer disease — relationship to biomarkers and genetics. *Nature Reviews Neurology*, 17(9):545–563.

Appendix A: C^* -algebraic formulation of quantum statistical mechanics

We recall here basic notions from the theory of C^* -algebras and the mathematical formulation of quantum statistical mechanics used in the main text. Readers interested in more details on the subject might refer to any classic references such as Dixmier’s [23] and [14].

§1. C^* -algebras. A C^* -algebra is Banach space \mathcal{O} which is an algebra over \mathbb{C} equipped with an involution

$$\mathcal{O} \longrightarrow \mathcal{O}, \quad A \mapsto A^*,$$

such that

$$(i) \quad \|AB\| \leq \|A\| \|B\| \text{ for all } A, B \in \mathcal{O}, \text{ and}$$

$$(ii) \quad \|A^*A\| = \|A\|^2 \text{ for all } A \in \mathcal{O}.$$

We say \mathcal{O} is *unital* if it has a unit element 1. An element $A \in \mathcal{O}$ is *self-adjoint* if $A^* = A$. And A is said to be *positive* if $A = B^*B$ for some $B \in \mathcal{O}$. In such a case, one writes $A \geq 0$. Moreover, we write $A \geq B$ if $A - B$ is positive in \mathcal{O} .

For instance the matrix algebra $\mathcal{O} = M_n(\mathbb{C})$ is a unital C^* -algebra where the involution is given by $A^* = A^\top$, for $A \in M_n(\mathbb{C})$, and 1 is the identity matrix. More generally, the algebra $B(\mathcal{H})$ of bounded linear operators on a Hilbert space \mathcal{H} is a C^* -algebra with respect to the operator norm $\|\cdot\|_{op}$ given by

$$\|T\|_{op} = \sup\{\|T\xi\| : \xi \in \mathcal{H}, \|\xi\| \leq 1\}.$$

An operator $T \in B(\mathcal{H})$ is positive if and only if $\langle T\xi, \xi \rangle \geq 0$ for all $\xi \in \mathcal{H}$.

§2. States. A linear functional $\sigma : \mathcal{O} \rightarrow \mathbb{C}$ is said to be *positive* if $\sigma(A^*A) \geq 0$ for all $A \in \mathcal{O}$. A *state* on a C^* -algebra \mathcal{O} is a positive linear functional σ such that $\|\sigma\| = 1$. A *trace-state* on \mathcal{O} is a state σ satisfying $\sigma(AB) = \sigma(BA)$.

For example, the usual trace of a matrix is a trace-state on $M_n(\mathbb{C})$, which shows that the notion of state is, in fact, a generalization of the trace functional.

§3. C^* -dynamical systems. The mathematical formalism of quantum statistical mechanics in the realm of C^* -algebras [14, 34, 35] and noncommutative geometry [18] can be summarized as follows. A quantum system is represented by a pair (\mathcal{O}, α) , called a *C^* -dynamical system*, consisting of C^* -algebra \mathcal{O} of observables, and the time evolution $(\alpha_t)_{t \in \mathbb{R}}$ of the system, which is a one-parameter group of $*$ -automorphisms of \mathcal{O} ; that is, α is a continuous map from \mathbb{R} to the automorphism group of \mathcal{O} that respects the C^* -algebra structure [23]. In the finite dimensional case where \mathcal{O} is a matrix algebra $M_n(\mathbb{C})$, the one-parameter group of $*$ -automorphisms in a C^* -dynamical system $(M_n(\mathbb{C}), \alpha)$ is necessarily an action of the form

$$\alpha_t(A) = e^{itH} A e^{-itH}, \quad t \in \mathbb{R}, A \in M_n(\mathbb{C}), \quad (\text{A1})$$

where $H \in M_n(\mathbb{C})$ is a self-adjoint matrix, and we recover the usual Hamiltonian of a quantum system [31].

Now given a state σ on \mathcal{O} , one might think of the element $\sigma(A)$ as the expectation value of the observable A when the system is in state σ . By analogy, the physical interpretation of $\sigma(\alpha_t(\cdot))$ is that the system is in state $\sigma \circ \alpha_t$ at time t if it was in state σ at time 0.

§4. KMS states. The thermal equilibrium states of the system at a given inverse temperature $\beta = \frac{1}{T}$ are mathematically characterized by the *Kubo-Martin-Schwinger (KMS)* conditions [30, 77]. Specifically, a state σ on \mathcal{O} is a KMS equilibrium state at inverse temperature β on (\mathcal{O}, α) , or a β -KMS state in short, if

$$\sigma(A\alpha_{i\beta}(B)) = \sigma(BA), \quad (\text{A2})$$

for all analytic elements A, B in (\mathcal{O}, α) , where an element $A \in \mathcal{O}$ is said to be *analytic* in the C^* -dynamical system if the function $t \mapsto \alpha_t(A)$ extends to an analytic function

$$\mathbb{C} \rightarrow \mathcal{O}, \quad z \mapsto \alpha_z(A).$$

It is immediate that a β -KMS state σ is necessarily time-invariant with respect to the dynamics α ; that is, $\sigma(\alpha_t(A)) = \sigma(A)$ for all $A \in \mathcal{O}$. In particular, 0-KMS states are *trace-states* (see Appendix A) that are time-invariant, and they represent the equilibrium states of the system at infinite temperature. And at the other extreme, ∞ -KMS states correspond to the *ground states* of the systems [14, 30].

§5. Relation to Gibbs states. For example, in the finite-dimensional case, for any non-negative inverse temperature β , the C^* -dynamical system $(M_n(\mathbb{C}), \alpha)$ has a unique β -KMS equilibrium state given by the Gibbs state [31]

$$\sigma_\beta(A) = \frac{\text{Tr}(e^{-\beta H} A)}{\text{Tr}(e^{-\beta H})}. \quad (\text{A3})$$

Appendix B: Directed networks as quantum systems

§6. Directed networks. A directed network G consists of a finite set of nodes $V = \{u, v, \dots\}$, and a finite set of directed edges $E = \{e, f, \dots\}$ between pair of nodes. If e is edge from v to u , we say that e has *source* $s(e) = v$ and *range* $r(e) = u$. We allow G to be a '*multigraph*'; that is, there might be more than one edge with source v and range u (parallel edges), and it is possible to have edges from one node to itself (self-loops). Figure 7 shows an example of such graphs. A *walk* (or a *path*) of length n is a sequence \mathbf{e} of edges e_1, \dots, e_n such that $s(e_i) = r(e_{i+1})$ for $i = 1, \dots, n-1$; we then write $|\mathbf{e}| = n$, $s(\mathbf{e}) = s(e_n)$, and $r(\mathbf{e}) = r(e_1)$. We let $N = \#V$ be the number of nodes of G , and define the *adjacency matrix* $A \in M_V(\mathbb{N})$ of G by

$$A_{uv} := \#\{e : s(e) = v, r(e) = u\}. \quad (\text{B1})$$

Observe that for a non-negative integer k , A_{uv}^k is the number of directed walks of length k from v to u .

§7. The graph C^* -algebra. An efficient and elegant way to study the combinatorial and topological properties of a directed network is to view its nodes and edges as bounded linear operators on a Hilbert space, and use these to generate a C^* -algebra encoding all the possible routes within the graph. Specifically, one can represent a directed

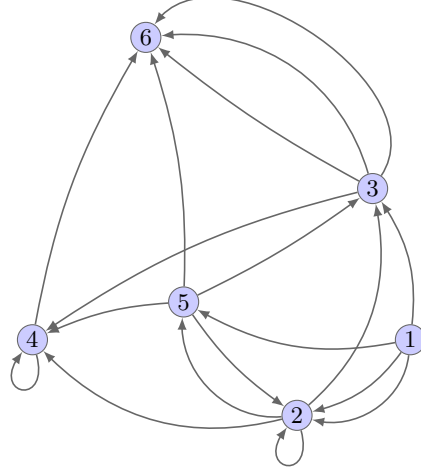


FIG. 7: **Directed networks.** Schematic illustration of a directed network that is a multigraph of 6 nodes with multiple parallel edges and self-loops.

graph G by a C^* -algebra \mathcal{O}_G , the Toeplitz algebra of G [20, 45, 58], defined as the universal C^* -algebra generated by a family $\{P_v : v \in V\}$ of mutually orthogonal projections on a Hilbert space \mathcal{H} and a family $\{S_e : e \in E\}$ of partial isometries on \mathcal{H} satisfying the *Toeplitz-Cuntz-Krieger* conditions [45, 58]

$$\begin{aligned} S_e^* S_e &= P_{s(e)}, \text{ for all } e \in E, \\ \sum_{r(e)=v} S_e S_e^* &\leq P_v, \text{ for all } v \in V. \end{aligned} \quad (\text{B2})$$

By definition, \mathcal{O}_G is the completion of the space spanned by projections of the form $S_{\mathbf{e}} S_{\mathbf{f}}^*$ such that $s(\mathbf{e}) = s(\mathbf{f})$, where for a walk $\mathbf{e} = (e_1, \dots, e_n)$, $S_{\mathbf{e}} := S_{e_1} \cdots S_{e_n}$. One can easily check that the sum $\sum_{v \in V} P_v$ is a unit element in \mathcal{O}_G , which makes it a unital C^* -algebra.

§8. C^* -dynamics on the graph C^* -algebra. There is a natural one-parameter group of $*$ -automorphisms $(\alpha_t)_{t \in \mathbb{R}}$ on \mathcal{O}_G given by

$$\begin{aligned} \alpha_t(P_v) &= P_v, \quad v \in V, \\ \alpha_t(S_e) &= e^{it} S_e, \quad e \in E, \end{aligned} \quad (\text{B3})$$

thus defining a quantum system represented by the C^* -dynamical system (\mathcal{O}_G, α) .

§9. KMS states on \mathcal{O}_G . We are now interested in the KMS states of the system (\mathcal{O}_G, α) . In fact, it can be seen [3, 38] that for an inverse temperature $\beta > 0$, the KMS condition (A2) for a state σ on this system is equivalent to the following relation

$$\sigma(S_{\mathbf{e}} S_{\mathbf{f}}^*) = \delta_{\mathbf{e}, \mathbf{f}} e^{-\beta |\mathbf{e}|} \sigma(P_{s(\mathbf{e})}), \quad (\text{B4})$$

for all $\mathbf{e}, \mathbf{f} \in W(G)$. In particular, for all $e \in E$, we get

$$\sigma(S_e S_e^*) = e^\beta \sigma(P_{s(e)}). \quad (\text{B5})$$

It follows from B2 and B5 that if σ is a β -KMS state on \mathcal{O}_G , then for all node $v \in V$, we have

$$\begin{aligned} \sum_{r(e)=v} e^{-\beta} \sigma(P_{s(e)}) &\leq \sigma(P_v) \\ \sum_{r(e)=v} \sigma(P_{s(e)}) &\leq e^\beta \sigma(P_v). \end{aligned} \quad (\text{B6})$$

And by observing that

$$\begin{aligned} \sum_{r(e)=v} \sigma(P_{s(e)}) &= \sum_{u \in V} \sum_{s(e)=u, r(e)=v} \sigma(P_u) \\ &= \sum_u A_{vu} \sigma(P_u), \end{aligned}$$

and defining the vector $\mathcal{X}^\sigma \in \mathbb{R}_+^V$ by the non-negative numbers $\mathcal{X}_v^\sigma := \sigma(P_v)$, the inequalities (B6) translates as

$$\mathbf{A} \mathcal{X}^\sigma \leq e^\beta \mathcal{X}^\sigma, \quad (\text{B7})$$

for a β -KMS state σ , where the inequality is coordinate-wise. One might think of \mathcal{X}^σ as a 'sub-eigenvector' of \mathbf{A} for e^β .

§10. KMS states as probability distributions. Since the unit element 1 of \mathcal{O}_G is given by $\sum_v P_v$, we obtain

$$\|\mathcal{X}^\sigma\|_1 := \sum_v \mathcal{X}_v^\sigma = 1, \quad (\text{B8})$$

which implies that \mathcal{X}^σ defines a probability distribution on the nodes set V .

§11. Defining the emittance volume. Denote the spectral radius of \mathbf{A} by r_G and define the *critical inverse temperature* as $\beta_c = \log r_G$. As a consequence of Equation (B7), if $\beta > \beta_c$ and σ is a β -KMS state, then e^β is not an eigenvalue of \mathbf{A} and \mathcal{X}^σ is not an eigenvector of \mathbf{A} . Hence, the inequality becomes strict. It follows that for $\beta > \beta_c$ the vector

$$\Psi^\sigma := (1 - e^{-\beta} \mathbf{A}) \mathcal{X}^\sigma \quad (\text{B9})$$

is strictly positive. Therefore, we can write

$$\mathcal{X}^\sigma = (1 - e^{-\beta} \mathbf{A})^{-1} \Psi^\sigma \quad (\text{B10})$$

But since $e^{-\beta} r_G < 1$, it follows from the theory of functional analysis (see for instance [15, Chap. 1 & 5]) that

$$(1 - e^{-\beta} \mathbf{A})^{-1} = \sum_{k=0}^{\infty} e^{-\beta k} \mathbf{A}^k. \quad (\text{B11})$$

Hence, $\mathcal{X}^\sigma = \sum_k e^{-\beta k} \mathbf{A}^k \Psi^\sigma$. Now consider the coordinate-wise non-negative vector \mathcal{Y}^β indexed over the nodes set V and given by

$$\mathcal{Y}_v^\beta = \sum_{s(\mathbf{e})=v} e^{-\beta |\mathbf{e}|}.$$

To see that these quantities are well defined, observe that the right-hand side can be written as

$$\begin{aligned} \sum_{s(\mathbf{e})=v} e^{-\beta |\mathbf{e}|} &= \sum_k \sum_{|\mathbf{e}|=k, s(\mathbf{e})=v} e^{-\beta k} \\ &= \sum_k \sum_{u \in V} e^{-\beta k} A_{uv}^k \\ &= \sum_{u \in V} \sum_k e^{-\beta k} A_{uv}^k, \end{aligned}$$

and, thanks to (B11), this infinite series converges to $\sum_{u \in V} (1 - e^{-\beta} \mathbf{A})_{uv}^{-1}$ when $\beta > \beta_c$. This prompts us to define the *emittance volume* of a node at inverse temperature $\beta > \beta_c$, as

$$\mathcal{Y}_v^\beta = \sum_{u \in V} (1 - e^{-\beta} \mathbf{A})_{uv}^{-1}. \quad (\text{B12})$$

We think of \mathcal{Y}_v^β as the volume of all transmissions coming from v at inverse temperature β , given that the functioning of each link in the network is affected by a factor of $e^{-\beta}$.

§12. From the graph algebra to the underlying network. Now, the inner product $\Psi^\sigma \cdot \mathcal{Y}^\beta$ equals $\|\mathcal{X}^\sigma\|_1 = 1$. Indeed, using (B11), we have

$$\begin{aligned}
\sum_v \mathcal{X}_v &= \sum_v \sum_k \sum_u e^{-\beta k} \mathbf{A}_{vu}^k \Psi_u^\sigma \\
&= \sum_u \Psi_u^\sigma \left[\sum_v \sum_k e^{-\beta k} \mathbf{A}_{vu}^k \right] \\
&= \sum_u \Psi_u^\sigma \left[\sum_{s(\mathbf{e})=u} \sum_k e^{-\beta|\mathbf{e}|} \right] \\
&= \sum_u \Psi_u^\sigma \mathcal{Y}_u^\beta \\
&= \Psi^\sigma \cdot \mathcal{Y}^\beta \\
&= 1.
\end{aligned}$$

This proves that the distribution \mathcal{X}^σ associated with the β -KMS state σ is completely determined, through (B10), by the vector Ψ^σ that is a solution of the following equation.

$$\Psi \cdot \mathcal{Y}^\beta = 1. \quad (\text{B13})$$

Conversely, it was proved by an Haef *et al.* [3] that for any non-negative vector $\Psi \in \mathbb{R}_+^N$ satisfying (B13), with $\beta > \beta_c$, there is a β -KMS state $\sigma = \sigma_\Psi$ given by

$$\sigma(S_{\mathbf{e}} S_{\mathbf{f}}^*) = \delta_{\mathbf{e}, \mathbf{f}} e^{-\beta|\mathbf{e}|} \mathcal{X}_{s(\mathbf{e})},$$

where $\mathcal{X} \in \mathbb{R}_+^V$ is given by $\mathcal{X} = (1 - e^{-\beta} \mathbf{A})^{-1} \Psi$ as in formula (B10). Furthermore, this process defines a one-to-one correspondence between the set of such vectors Ψ and the β -KMS states on \mathcal{O}_G .

As a consequence of these constructions, we might think of the directed network G as a quantum system whose thermal equilibrium states are the probability distributions obtained from the KMS states of the C^* -dynamical system (\mathcal{O}_G, α) .

§13. The state spaces of a directed network. For a fixed $v \in V$ and $\beta > \beta_c$, define the vector $\Psi^{v,\beta} \in [0, \infty)^V$ as

$$\Psi^{v,\beta} = \left(\frac{1}{\mathcal{Y}_v^\beta} \delta_{u,v} \right)_{u \in V}. \quad (\text{B14})$$

It is obvious that these vectors satisfy equation (B13). Hence, we get for each fixed $v \in V$, a β -KMS state $\mathcal{Z}^v = \mathcal{Z}^{v,\beta}$ given by

$$\mathcal{Z}_u^v = \left((1 - e^{-\beta} \mathbf{A})^{-1} \Psi^{v,\beta} \right)_u = \frac{1}{\mathcal{Y}_v^\beta} \sum_k e^{-\beta k} \mathbf{A}_{uv}^k.$$

Or in a more compact form,

$$\mathcal{Z}_u^v = \frac{1}{\mathcal{Y}_v^\beta} (1 - e^{-\beta} \mathbf{A})_{uv}^{-1}. \quad (\text{B15})$$

\mathcal{Z}_u^v is a *Gibbs distribution* that gives the probability for a transmission (or a random walker) from v to reach u , given that the system is at inverse temperature β . In particular, \mathcal{Z}_v^v measures the probability that, when the system is at inverse temperature β , a transmission coming from v returns back to v .

It can be seen that the state space S_β of all β -KMS states on G is the simplex [67] of dimension $N - 1$ generated by the vectors $\mathcal{Z}^{v,\beta}$; that is,

$$S_\beta = \left\{ \sum_v p_v \mathcal{Z}^v \mid 0 \leq p_v \leq 1, \sum_v p_v = 1 \right\}. \quad (\text{B16})$$

Thus, the vectors $\mathcal{Z}^{v,\beta}$ are the *pure* (β -KMS) states of the system, while their convex combinations are *mixed states* [14]. In a sense, the states \mathcal{Z}^v are the analog of the eigenvectors and the simplex S_β plays the role of eigenspace. It follows that every β -KMS state \mathcal{X} can be written as a matrix product

$$\mathcal{X} = \mathbf{Z}^\beta P, \quad (\text{B17})$$

where $P = (p_v)_v$ is a probability distribution on V and \mathbf{Z}^β is the stochastic $N \times N$ -matrix with non-negative entries whose columns are the vectors \mathcal{Z}^v ; that is, $\mathbf{Z}_{uv}^\beta := \mathcal{Z}_u^{\beta,v}$.

Appendix C: Connectivity states of the *C. elegans* directed connectome

In this note, we apply the theory presented above to the directed multigraph defined by the somatic connectome of the nematode *C. elegans*.

§14. The directed connectome. We merged two datasets of the somatic connectome of the hermaphrodite worm *C. elegans* that are publicly available on the WormAtlas [2]: the first one (*Data1*) is from Varshney et al. [71], and the second one (*Data2*) is from the recently published serial electron microscopy reconstructions of the whole connectome by Cook et al. [19]. Specifically, we kept all synaptic connections from *Data1* (279 connected neurons and 8171 chemical and electrical synapses), and all synaptic connections in *Data2* that were not originally in *Data1* (3900 additional connections) were merged into *Data1*. The resulting connectome consists of 280 connected neurons and 12071 synaptic connections. In this revised connectome, 44 neurons have 'autapses'; i.e., the synapse onto themselves. We then represent this connectome as a directed network G (Figure 8) with parallel edges and self-loops whose node set V consists of the neurons and edge set E represents the chemical and electrical transmissions among those: chemical synapses are represented as unidirectional edges between neurons (oriented arrows) $v \xrightarrow{e} u$, and gap-junctions are represented as two reciprocal links between neurons $v \xrightleftharpoons[f]{e} u$.

§15. Connectivity state vectors, receptance, and the weighted structural connectome. By a *connectivity state vector* we mean a probability distribution \mathcal{X} on V such that, for $u \in V$, \mathcal{X}_u represents a probability of upstream connectivity of u . We call \mathcal{X}_u the *receptance* of u when *the system is in state* \mathcal{X} .

For example, for each fixed $v \in V$, define the *structural connectivity* state vector \mathcal{K}^v by $\mathcal{K}_u^v = A_{uv} / \sum_w A_{wv}$. This is clearly a connectivity state vector in which the receptance of u is the synaptic density from v to u .

Now let $\underline{\mathcal{K}}^v$ be the vector defined by setting

$$\underline{\mathcal{K}}_v^v = 0, \text{ and } \underline{\mathcal{K}}_u^v = \frac{\mathcal{K}_u^v}{\sum_{w \neq v} \mathcal{K}_w^v} \text{ if } u \neq v \text{ and } \mathcal{K}_u^v > 0. \quad (\text{C1})$$

We let the *weighted structural connectome* be the weighted directed graph \mathcal{K} whose adjacency matrix has columns the vectors $\underline{\mathcal{K}}^v$. Specifically, \mathcal{K} is the simple weighted graph representing the connectome with all autapses removed and parallel synapses replaced by their relative weights; i.e., the weight of a connection from v to u is the ratio of the number of synapses from v to u out of the number of all outgoing synapses from v .

§16. Neural emittance profiles. Applying the theory of KMS states on the quantum system defined by G , the critical inverse temperature is $\beta_c = 4.2958$. For $\beta > \beta_c$ and neuron v , we refer to the pure β -KMS state $\mathcal{Z}^{v,\beta}$ as the *neural emittance profile* of v at inverse temperature β , or simply the NEP_β of v . The NEP_β of a v is clearly a connectivity state vector, and the receptance of a neuron u in this state is referred to as the *neural β -emittance* of u from v .

§17. Emittance networks. We use similar formula as (C1) to represent these vectors as directed weighted networks: we let $\underline{\mathcal{Z}}^{v,\beta}$ be defined by

$$\underline{\mathcal{Z}}_v^{v,\beta} = 0, \text{ and } \underline{\mathcal{Z}}_u^{v,\beta} = \frac{\mathcal{Z}_u^{v,\beta}}{\sum_{w \neq v} \mathcal{Z}_w^{v,\beta}} \text{ if } u \neq v \text{ and } \mathcal{Z}_u^{v,\beta} > 0. \quad (\text{C2})$$

The components of $\underline{\mathcal{Z}}^{v,\beta}$ quantify the degree to which neuron v 'functionally' connects onto every other neuron in the connectome when the system is at inverse temperature β . The vector can then be represented as a weighted directed star called the *emittance network* of v at inverse temperature β .

§18. Structure-function divergence and functional temperatures. In order to measure the degree to which the emittance networks of a neuron v differ from its structural connectivity network, we introduce the *structure-function*

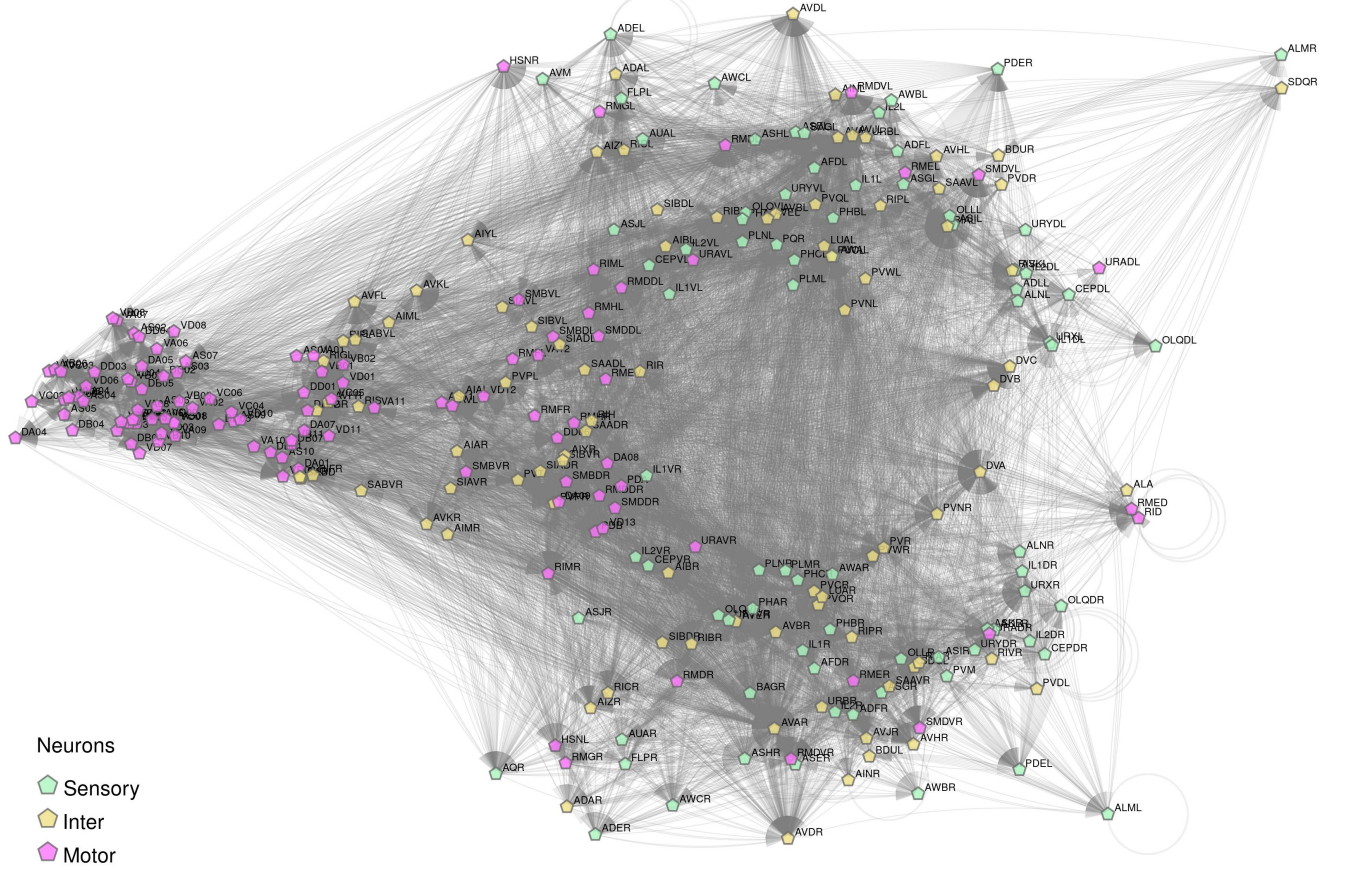


FIG. 8: **The *C. elegans* connectome.** The directed multigraph G representing the synaptic wiring of the somatic nervous system of the *C. elegans*. It consists of 280 nodes (neurons) and 12071 directed edges representing the chemical and electrical transmissions between neurons.

divergence (**sfd**) as follows:

$$\mathbf{sfd}(v, \beta) = 1 - \left(\sum \left(\kappa_u^v z_u^{v, \beta} \right)^{1/2} \right)^2. \quad (\text{C3})$$

Specifically, **sfd** measures how the two networks representing the NEP_β diverges from the anatomical wiring of the neuron in terms of both the number and intensity of their respective connections. Namely, it provides the ratio of non-overlapping receptances in both state vectors.

Figure 9 shows that for some neurons the emittance networks deviate quickly and significantly from structural connectivity, while for others they remain close to structural connectivity for long temperature intervals. In particular, the motor neuron AS08 has globally the highest **sfd**, while the command interneurons AVAL/R have among the lowest (see Figure 10).

Moreover, observe from Figure 9 that most neurons have their **sfd** are either close to zero or relatively low for temperature values close to $1/\beta_s$. It is then reasonable to assume that the emittance networks at temperatures between $1/\beta_s$ and some value $1/\beta_f$ do not give functional and computational information beyond what is provided by structural connectivity. In order to determine β_f , we consider the *mean total receptance* of the connectome defined as follows

$$\mathbf{mtr}(\beta) = \frac{\sum_v \sum_{u \neq v} z_u^{v, \beta}}{N(N-1)}, \quad (\text{C4})$$

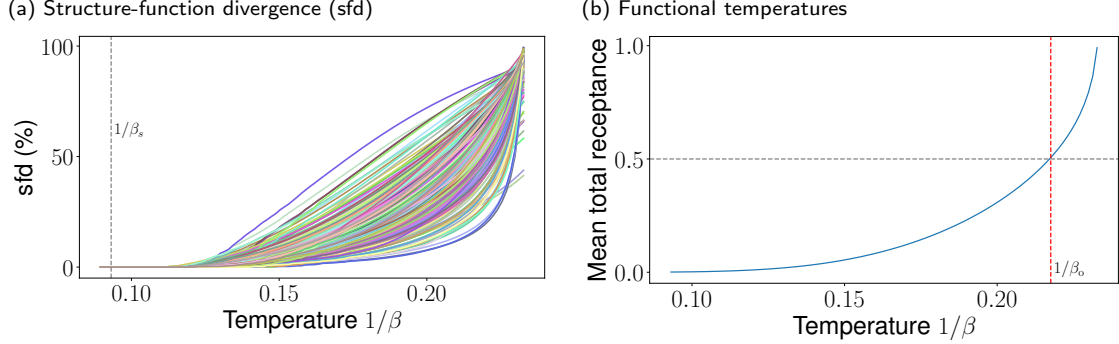


FIG. 9: **Structural and functional temperatures.** (a) Graphical illustration of the variation of the structure-function divergence (sfd) of all neurons with respect to the β values. sfd measures how much the emittance network of a neuron at inverse temperature β differs from its structural connectivity. The structural (inverse) temperature β_s is the value of β that minimizes the sfd of all neurons. (b) The mean total receptance gives the average total receptance in the pure states. At $\beta_o = 1.07\beta_c$, this quantity is 0.5, meaning that on average neurons receives more flows from other neurons than from themselves through self-emittance. We see that for temperature values above $1/\beta_o$, the mean total receptance is > 0.5 ; these are the 'functional temperatures' as they allow more communications between different neurons.

which measures the average proportion of information flow a neuron receives from all the other neurons at inverse temperature β excluding its feedback loops. For instance, $\mathbf{mtr}(\beta) = 0.5$ implies that, on average, 50% of all the total incoming information flow of a neuron at this inverse temperature come exclusively from the other neurons, and therefore the other 50% originate from the neuron itself (through cycles). Our working convention is that a β value is 'functional' if $\mathbf{mtr}(\beta) > 0.5$, or in other words, if on average, a neuron receives more information flows from the other neurons than from itself (see Figure 9b). And letting β_o be such that $\mathbf{mtr}(\beta_o) = 0.5$, we get $\beta_o = 1.07\beta_c$, and therefore, $I_f = (\beta_c, 1.07\beta_c)$ is the 'functional' inverse temperature interval.

§19. β -connectivity matrices. Equation (B17) shows that all mixed states are determined by a probability measure on V and the matrix \mathbf{Z}^β . For the sake of simplicity, one can view \mathbf{Z}^β as the matrix with column vectors $\underline{\mathcal{Z}}^{v,\beta}$ instead of $\mathcal{Z}^{v,\beta}$. We then call \mathbf{Z}^β the β -connectivity matrix of the connectome, as its entries are measure of interconnectivity between neurons when the system is at inverse temperature β . More precisely, each entry $\mathbf{Z}_{u,v}^\beta$ measure the degree to which the neuron v functionally connects onto neuron u by considering all the possible routes connecting them when the system is at inverse temperature β .

§20. Statistical significance and dependence of neural emittance on network topology. By definition, neural emittance profiles provides measures of information pathways between neurons. One question that naturally arises is to what extent these measures are dictated by the specific wiring of the connectome. In other words, which of these measures would significantly change if the system is randomly rewired while each neuron keeps the same number of incoming and outgoing connections? To address this question, we generated random directed multigraphs G_n ($n = 1, \dots, 5000$) with the same degree sequence as G , and at a given temperature β and a fixed neuron v , computed $\underline{\mathcal{Z}}^{v,\beta}$ in each G_n , and then compared their values with that of the $\underline{\mathcal{Z}}^{v,\beta}$ obtained from the original graph G . If a receptance appears with low frequency in these graphs ($p < 0.05$) with a value that is equal to or larger than its corresponding value in the original graph G , we consider this receptance as dependent on the network topology, meaning that it is directly predicted from the specific anatomical wiring of the connectome. We refer to the weighted connection corresponding to such a measure within the emittance network as a *pure functional connection* (PFC).

§21. The pure functional connectome. In order to get a complete atlas of all the pure functional connections of the connectome at a given β value, we restrict the β -connectivity matrix \mathbf{Z}^β to its entries that are statistically significant, and then normalize the column vectors of the resulting matrix. We then obtain the adjacency matrix of the directed weighted graph whose nodes are all the neurons and edges are all the functional connections predicted from the network topology of the *C. elegans* connectome. We call this network the *pure functional connectome* at inverse temperature β , and denoted it as \mathcal{F}^β . Figure 11 represents \mathcal{F}^β at the functional value of $\beta_f = 1.05\beta_c$.

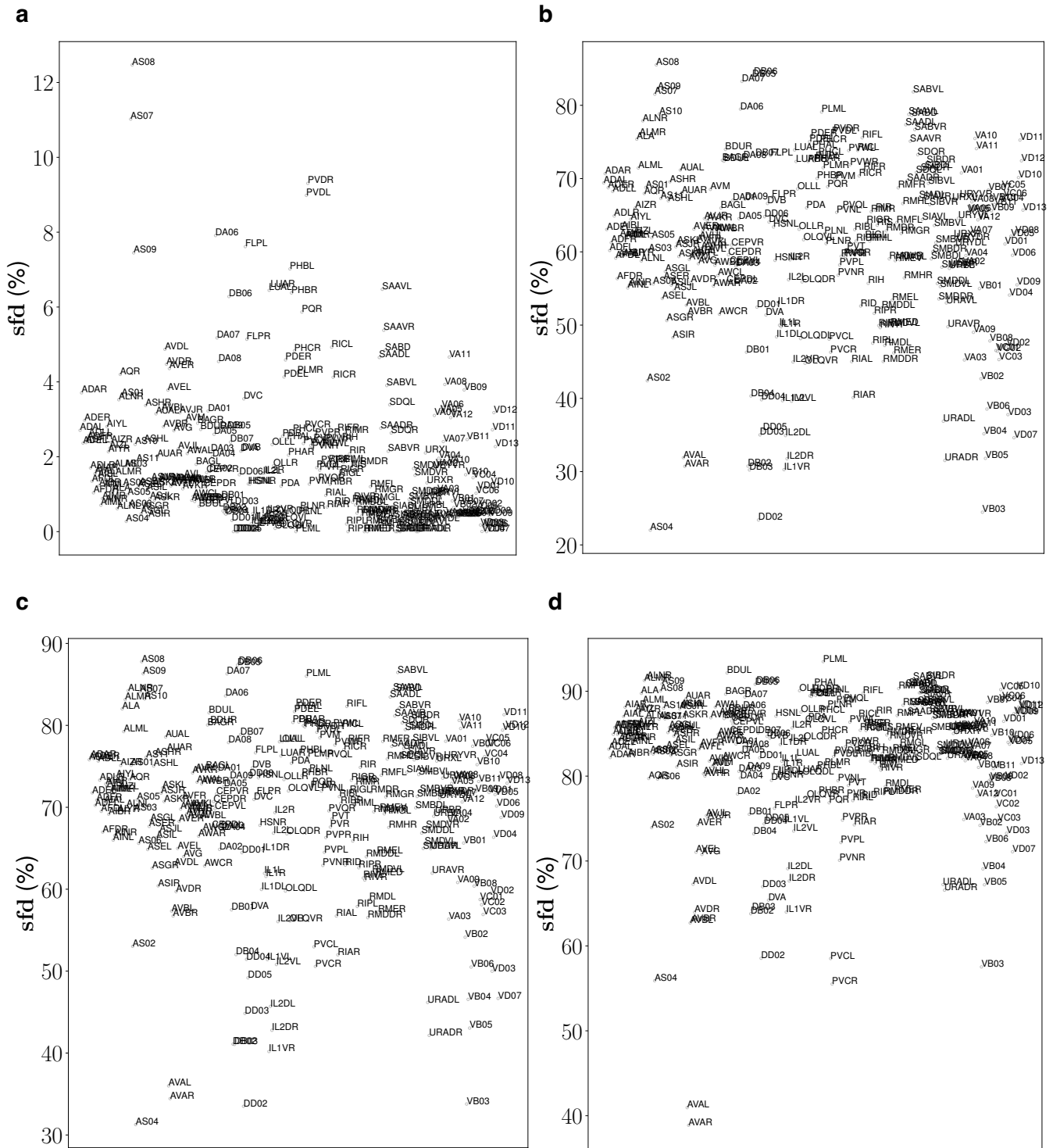


FIG. 10: *sfd* variation. Schematic representing of all neurons according to their *sfd* in percentage at different β values. **a:** $\beta = 1.7\beta_c$. **b:** $\beta = 1.05\beta_c$. **c:** $\beta = 1.03\beta_c$. **d:** $\beta = 1.01\beta_c$.

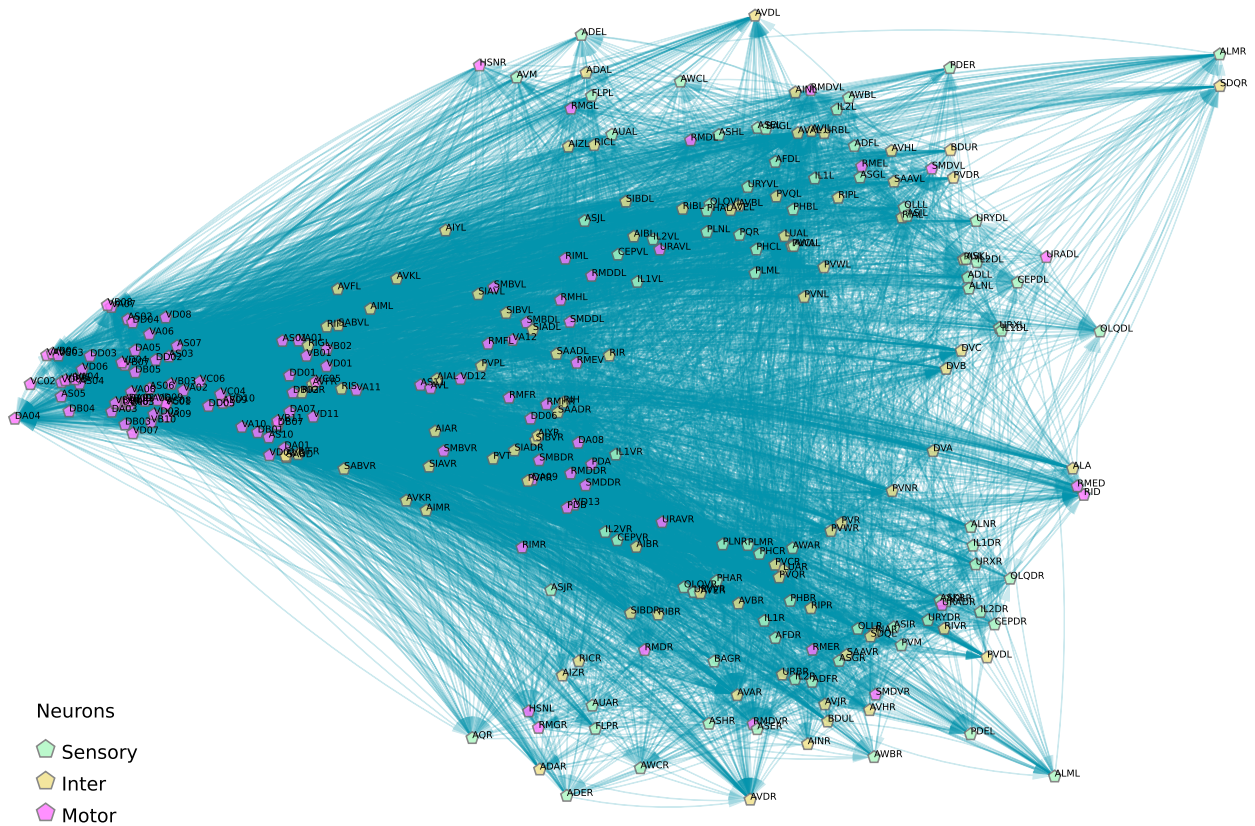


FIG. 11: **Pure functional network.** Schematic of the pure functional connectome \mathcal{F}^β of the *C. elegans* at a functional inverse temperature value $\beta_f = 1.05\beta_c$. It represents only 11.68% of the whole directed weighted network defined by the matrix \mathbf{Z}^β whose column vectors are the neural β -emittance profiles of all neurons. Neurons are positioned according to their spatial coordinates [63].

Appendix D: Classification of neurons by integration capacity

TABLE III: Neuron classification by integration capacity

Group 1	<p>ADER, AS01, AS02, AQR, ALNR, ALMR, AS03, AS04, AS05, AS06, AS07, AS08, AS09, AS10, AS11, ASHR, AVAL, AVAR, AVBR, AVBL, AVDL, AVDR, AVEL, AVER, AVG, AVHL, AVHR, AVJL, AVJR, AVKL, AVL, AVM, DA01, DA02, DA03, DA04, DA05, DA06, DA07, DA08, DA09, DB01, DB02, DB03, DB04, DB05, DB06, DB07, DD01, DD02, DD03, DD04, DD05, DD06, DVA, DVB, DVC, FLPL, FLPR, LUAL, LUAR, PDA, PDB, PDEL, PDER, PHBL, PHCL, PHCR, PLML, PLMR, PQR, PVCL, PVCR, PVDL, PVDR, PVM, PVNL, PVNR, PVPL, PVPR, PVR, PVT, PVWL, PVWR, RID, RIMR, SAAVR, SABD, SABVL, SABVR, SDQL, SDQR, SIBDL, SIBVL, URYDL, URYDR, URYVL, URYVR, VA01, VA02, VA03, VA04, VA05, VA06, VA07, VA08, VA09, VA10, VA11, VA12, VB01, VB02, VB03, VB04, VB05, VB06, VB07, VB08, VB09, VB10, VB11, VC01, VC06, VD01, VD02, VD03, VD04, VD05, VD06, VD07, VD08, VD09, VD10, VD11, VD12, VD13</p>
Group 2	<p>ADLR, ADFR, ADFL, AFDL, AFDR, ADEL, ADLL, AIAL, AIAR, AIBL, AIBR, AIML, AIMR, AINL, AINR, AIYL, AIYR, AIZL, AIZR, ALML, ALNL, ASEL, ASER, ASGL, ASGR, ASHL, ASIL, ASIR, ASJL, ASJR, ASKL, ASKR, AUAL, AUAR, AWAL, AWAR, AWBL, AWBR, AWCL, AWCR, BAGL, BAGR, CEPDL, CEPDR, CEPVL, CEPVR, HSNL, IL1DL, IL1DR, IL1L, IL1R, IL1VL, IL1VR, IL2DL, IL2DR, IL2L, IL2R, IL2VL, IL2VR, OLLL, OLLR, OLQDL, OLQDR, OLQVL, OLQVR, RIAL, RIAR, RIBL, RIBR, RICL, RICR, RIH, RIPL, RIPR, RIVL, RIVR, RMDDL, RMDDR, RMDL, RMDR, RMDVL, RMDVR, RMED, RMEL, RMER, RMEV, RMGL, RMGR, RMHL, RMHR, SAADL, SAADR, SAAVL, SIADL, SIADR, SIAVL, SIAVR, SIBDR, SMBDL, SMBDR, SMBVL, SMDDL, SMDDR, SMDVL, SMDVR, URADL, URADR, URAVL, URAVR, URBL, URBR, URXL, URXR, VC02, VC03, VC04, VC05</p>
Group 3	<p>ADAR, ALA, AVFL, AVFR, AVKR, BDUL, BDUR, PHAL, PHAR, PHBR, RIGL, RIS, RMFL, RMFR, SIBVR, SMBVR</p>
Group 4	<p>ADAL, HSNR, PLNL, PLNR, PVQL, PVQR, RIFL, RIFR, RIGR, RIML, RIR</p>